

NASA CR 86259  
W69-40457

## FINAL TECHNICAL REPORT - PHASE II

# RESEARCH ON LOW VOLTAGE ELECTROLUMINESCENT DEVICES WITH STORAGE

J.M. HANLET

MARCH 1969

CONTRACT NO. NAS 12-545

CASE FILE  
COPY

Prepared By:  
**THE MARQUARDT COMPANY**  
CCI Aerospace Corporation  
16555 Saticoy Street  
Van Nuys, California

For:

**NATIONAL AERONAUTICS AND SPACE ADMINISTRATION**  
Electronics Research Center  
Cambridge, Massachusetts

Mr. Edwin Hilborn  
Technical Monitor  
NAS 12-545  
Electronics Research Center  
575 Technology Square  
Cambridge, Massachusetts 02139

"Requests for copies of this report should be referred to:

NASA Scientific and Technical Information Facility  
P. O. Box 33, College Park, Maryland 20740



RESEARCH ON LOW VOLTAGE ELECTROLUMINESCENT  
DEVICES WITH STORAGE

Jacques M. Hanlet

March 1969

Prepared under Contract No. NAS 12-545 by

THE MARQUARDT COMPANY  
CCI Aerospace Corporation  
Van Nuys, California

For:

NATIONAL AERONAUTICS AND SPACE ADMINISTRATION  
Electronics Research Center  
Cambridge, Massachusetts

TABLE OF CONTENTS

Summary	1
Introduction	2
Experimental Work	3
Background	3
Substrate Preparation	3
Vacuum Equipment	5
Vapor Deposition	10
Crystalline Structure	13
Electroluminescent Devices	26
Pin Structure	26
III-V - II-VI Structure	30
Conclusions	36
Appendix I	
Evaporating Sources Configuration	37
Experimental Work	42
Appendix II	
Chemistry of II-VI Compounds	44
References	53

### LIST OF ILLUSTRATIONS

<u>Figure</u>	<u>Page</u>
1 Etched Calcium Fluoride	4
2 Etched Sapphire	6
3 Vacuum System	7
4 Pressure vs. Pumping Time and System Configurations	8
5 Mass Spectrographic Analysis of Residuals	9
6 Mass Spectrography of Coevaporated Zn + Se	11
7 Equilibrium Concentration	12
8 Growth of ZnSe Layer Function of Molecular Fluxes	14
9 Film Composition vs. Se Flux at Zn Flux Constant	15
10 Zinc Selenide Diffraction Patterns	16
11 Epitaxial Growth on <0001> Sapphire	18
12 Epitaxial ZnSe Laue Patterns	19
13 Epitaxial ZnSe Laue Patterns	20
14 Epitaxial ZnSe Laue Patterns	21
15 Epitaxial ZnSe Laue Patterns	22
16 Epitaxial ZnTe Laue Patterns	23
17 Epitaxial ZnTe Laue Patterns	24
18 Capacitance vs. Voltage Across Junction	29
19 pin Diode Voltage - Current Relationship	31
20 pin Diode ZnSeGa Spectral Emission	32
21 Current - Brightness Relationship	33
22 Electroluminescent Model	34
23 Components of Evaporator Source Configuration	39
24 Assembled Evaporator Source Configuration	40
25 Evaporation Heater Source	41
26 Coaxial Circular Sources	50
27 Vapor Pressures of Vaporizing ZnTe	51

### LIST OF TABLES

I Clausing's Correction Factor for Source Geometry	49
II Sublimation and Partial Pressures of ZnSe	52

#### SUMMARY

During the course of this contract, monocrystalline films of ZnTe and ZnSe were produced over large areas by epitaxial deposition in vacuum.

A new method of chalcogene evaporation was originated which permits close control of the polymerism in the vapor state and thereby the point defect density.

Two forms of heterojunction were investigated and produced over large areas; both were operable at room temperature in scotopic conditions.

It can be concluded that as better hold on the II-VI compounds technology is gained, the greater the potential of their application will become towards useful electroluminescent devices.

## INTRODUCTION

The main goal of the contractual effort described in this report is to develop large host crystals and investigate the formation of electro-luminescent p-n junctions in II-VI compounds.

The latent interest in wide band gap compounds is mitigated by many difficulties in their exploitation. The principal obstacles pertain to sizes of crystals available, polymorphism, stoichiometric defects and self-compensation.

The small monocrystals dimensions control the range of practical devices, whereas light output and efficiency depend on the polymorphism, the point defects and self compensation.

Both polymorphism and point defects derive from processing technology and are susceptible to control, while self compensation is a characteristic of the II-VI compounds which cannot be disciplined.

Self compensation prevents amphoteric conductivity in all but one of the II-VI compounds viz. CdTe, which has a too narrow band gap for our purpose. As a result, low and unequal p & n carriers concentration preclude the formation of an efficient homojunction. Until such shortcomings are overcome less efficient electroluminescent devices can be expected from some form of heterojunction.

## EXPERIMENTAL WORK

### Background

The production of II-VI compounds in large monocrystals from the liquid phase is made difficult by the high vapor pressure of the elements at their melting point.<sup>(1)(2)</sup>

In the compounds of interest viz. ZnTe and ZnSe, the high temperature of formation<sup>(3)(4)</sup> imposes severe limitations on crucibles and containers usable for their growth<sup>(5)(6)</sup>. An alternative method used by growing the crystals from the vapor phase<sup>(7)(8)</sup> yields small crystals often presenting numerous dislocations and inclusions.

Since the thickness of any part of a junction is by necessity comparatively small, the epitaxial growth over large areas is obviously a tempting solution. The work published to date on epitaxial deposition is scarce and generally involves a substrate of identical specie<sup>(9)</sup>. In this particular reference one of the crystalline compounds is used as a substrate for epitaxing the other component from its vapor; this leaves the problem of area unresolved.

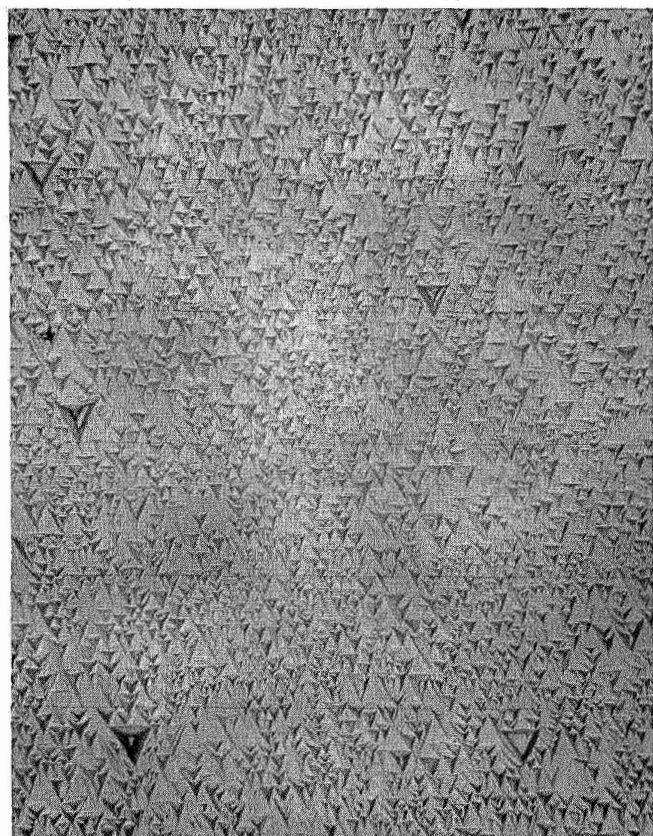
ZnTe has been deposited epitaxially from the vapor in vacuum<sup>(10)</sup> on LiF and CaF<sub>2</sub>, but films so produced are said to peel easily from their substrates.

### Substrates Preparation

Two types of substrate were extensively used during this work, CaF<sub>2</sub> crystals purchased from Isomet Corporation, Palisades Park, N. J., and Al<sub>2</sub>O<sub>3</sub> purchased from Union Carbide Corporation, Electronic Division, Torrance, California.

The same cleaning procedure was applied to all crystals prior to and after etching. The substrates were ultrasonically cleaned in Triton 100 X for 5 minutes, rinsed several times in deionized water, followed by alcohol rinse and forced air drying.

The CaF<sub>2</sub> crystals 1" x 1" x 0.25" were cleaved to around 0.040" thickness and etched in H<sub>3</sub>PO<sub>4</sub> heated at 165°C. The <111> etch pattern obtained after 20 minutes is shown in Figure 1. The CaF<sub>2</sub> crystals are very sensitive to thermal shock and great care had to be exercised in order to avoid shattering of the platelets. After cleaning the etched crystals and a careful rinse in water and alcohol, the substrates were immediately transferred to the vacuum chamber.



100X

Figure 1  
ETCHED CALCIUM FLUORIDE  
 $<111>$

R-26, 917

Two types of flame fusion sapphire crystals were purchased, 1" x 1" x 0.04" and disks of 0.5" diameter, 0.015" thick. They were respectively oriented in <1120> plane and for the disks in <0001> plane.

Occasional fine scratches, remaining from the diamond powder polish, were still visible under high magnification.

No etching was attempted on the <1120> cut crystals, while the <0001> were thermally etched in a fluorinated hydrocarbon vapor<sup>(11)</sup>.

The disks were placed on a carbon susceptor and introduced in a Vycor tube 1" I.D. The Vycor tube was fitted in a tubular furnace, well ventilated and heated progressively to 950°C, under a small flow of dry argon. When thermal equilibrium was achieved, a flow of 5 ml min<sup>-1</sup> of C<sub>2</sub>Cl<sub>2</sub>F<sub>4</sub> (Freon 114) from the Matheson Co., was introduced and the flow of argon cut off.

After cooling to room temperature, the cleaning procedure was again applied to the disks, prior to their introduction in the vacuum chamber.

A 35 minutes etch pattern of the <0001> cut is shown in Figure 2.

#### Vacuum Equipment

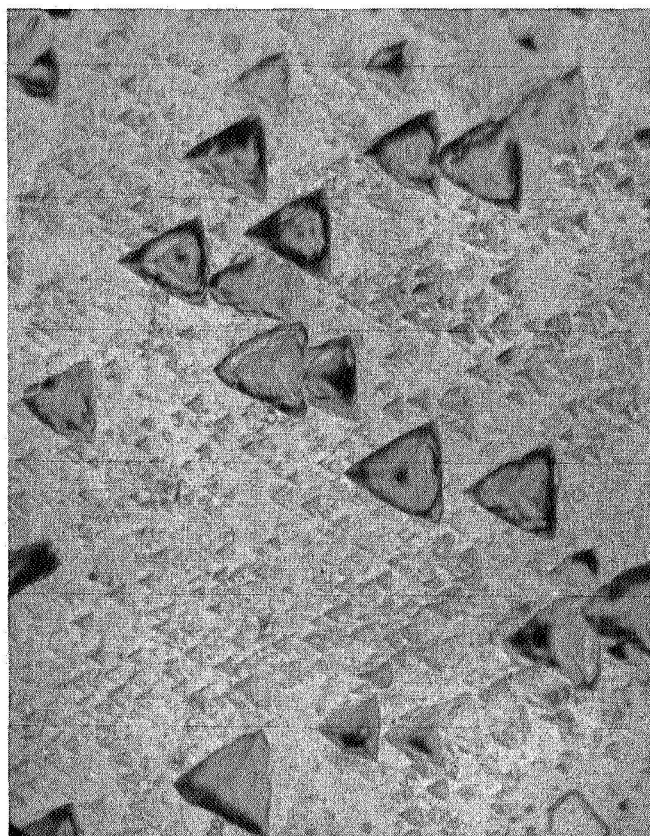
The vacuum system comprised a six inch diffusion pump with a double baffle, one water cooled the other cooled with liquid nitrogen.

Two additional pumps were attached to the 18" metallic belljar, both from Varian Associates, one a titanium sublimation pump and the other an 18 liters ion pump. A Veeco mass spectrometer was mounted on the side of the belljar with a high vacuum isolation valve of large aperture. The axis of the mass spectrometer made an angle of 30° with the normal to the coaxial gap of the evaporating sources, Figure 3.

After degassing the system for 8 to 10 hours at 150°C, the residual pressure, measured with a nude ion gauge, never exceeded 10<sup>-8</sup> torrs, in the vacuum enclosure, prior to each evaporation, Figure 4.

Besides N<sub>2</sub> and CO<sub>2</sub>, which are the main contributors to the background pressure, the residual gases consist mostly of the dienes C<sub>3</sub>H<sub>3</sub>, from cracking of the Corning 702 silicon oil. Figure 5 represents the mass and magnitude of the residue measured at 10<sup>-8</sup> torrs after thorough degassing.

The sources used for evaporation were of the type described previously (Referred to in Appendix I) except for minor modifications to the ionizing system. Instead of thermally ionizing the evolving chalcogene at around 3000°K, the temperature of the concentric filament was lowered to about 200° above the melt's temperature. A potential of approximately 300 volts was



200X

Figure 2  
ETCHED SAPPHIRE  
<0001>

R-26,918

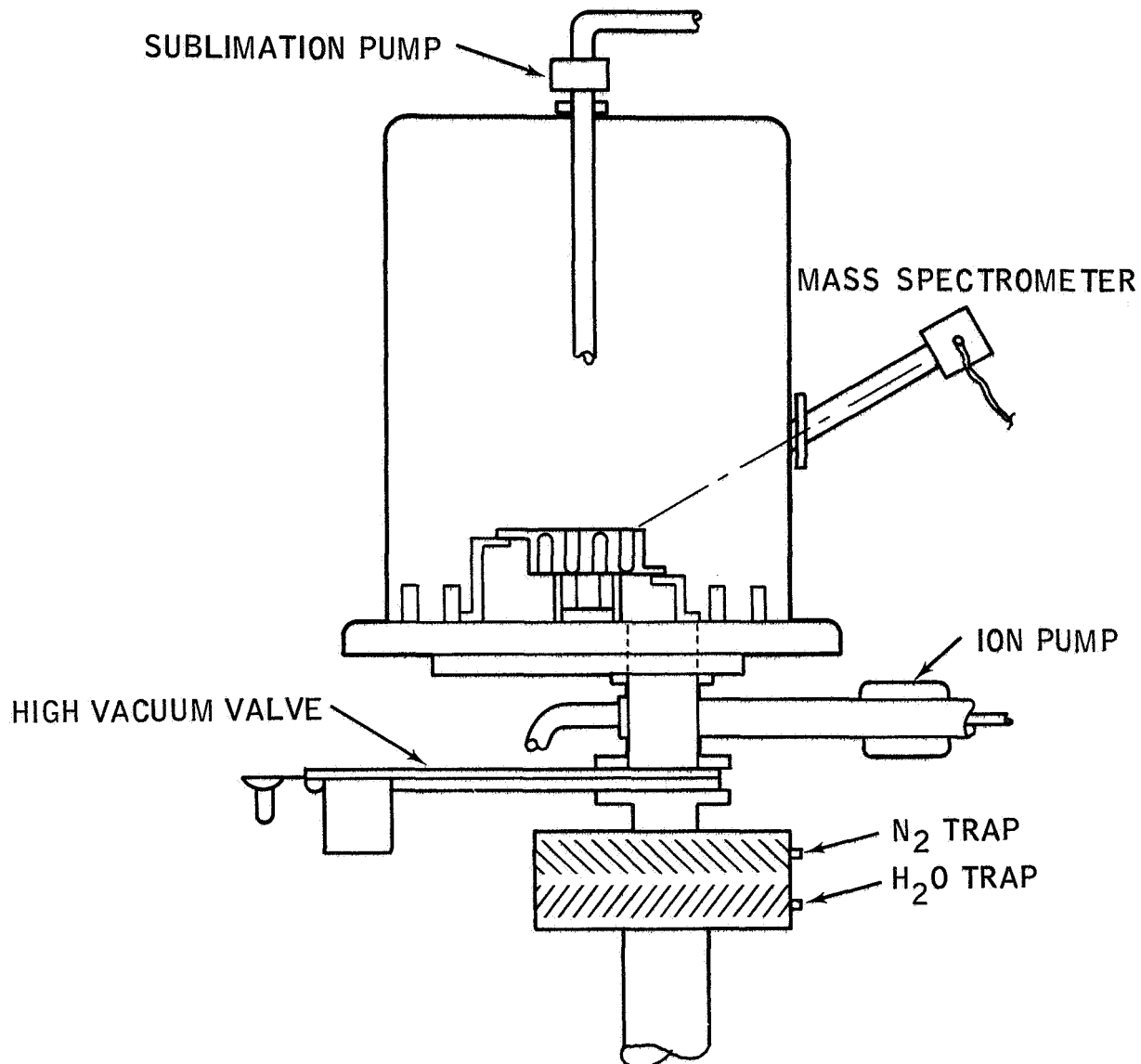


Figure 3  
VACUUM SYSTEM

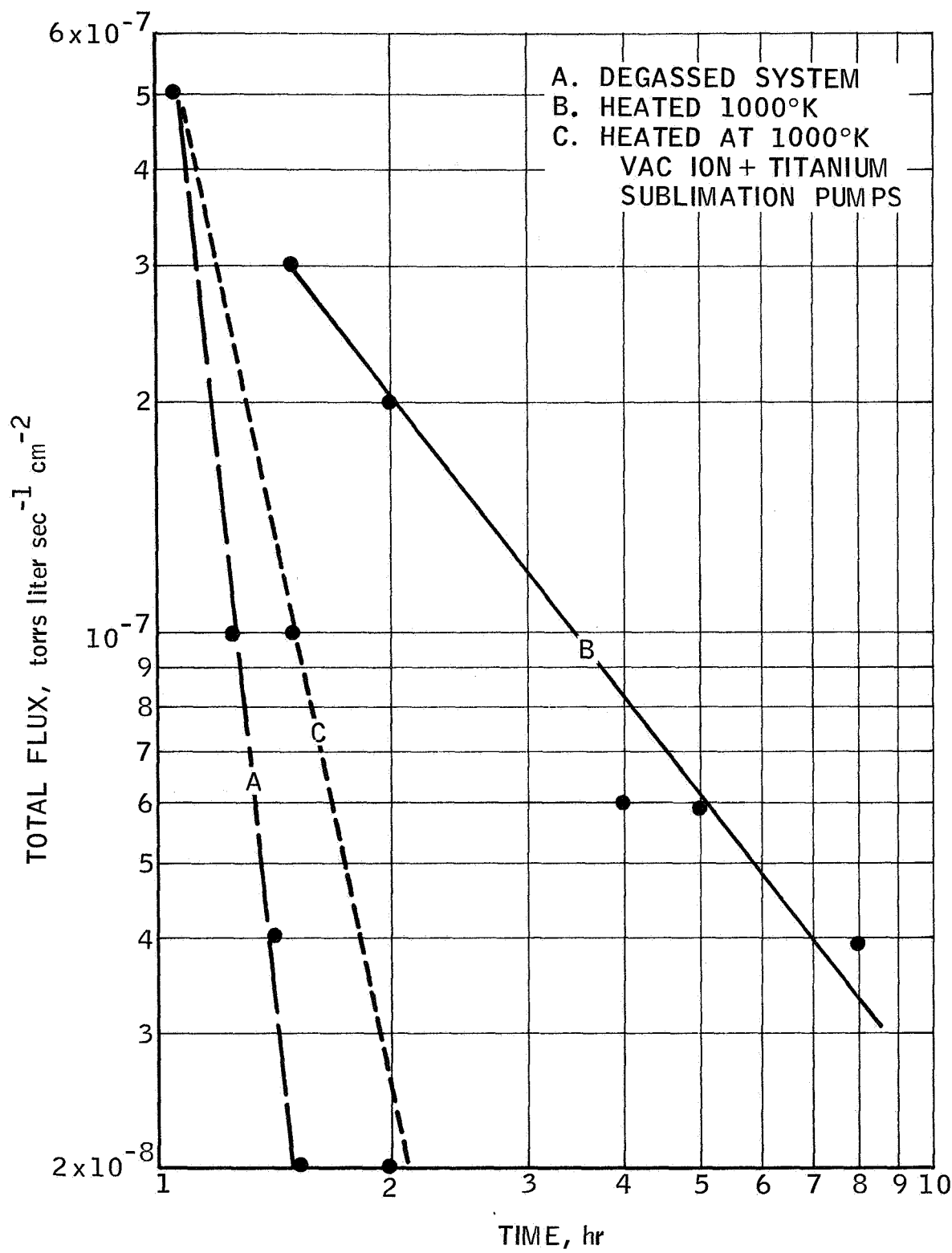


Figure 4  
 PRESSURE VS. PUMPING TIME  
 AND SYSTEM CONFIGURATIONS

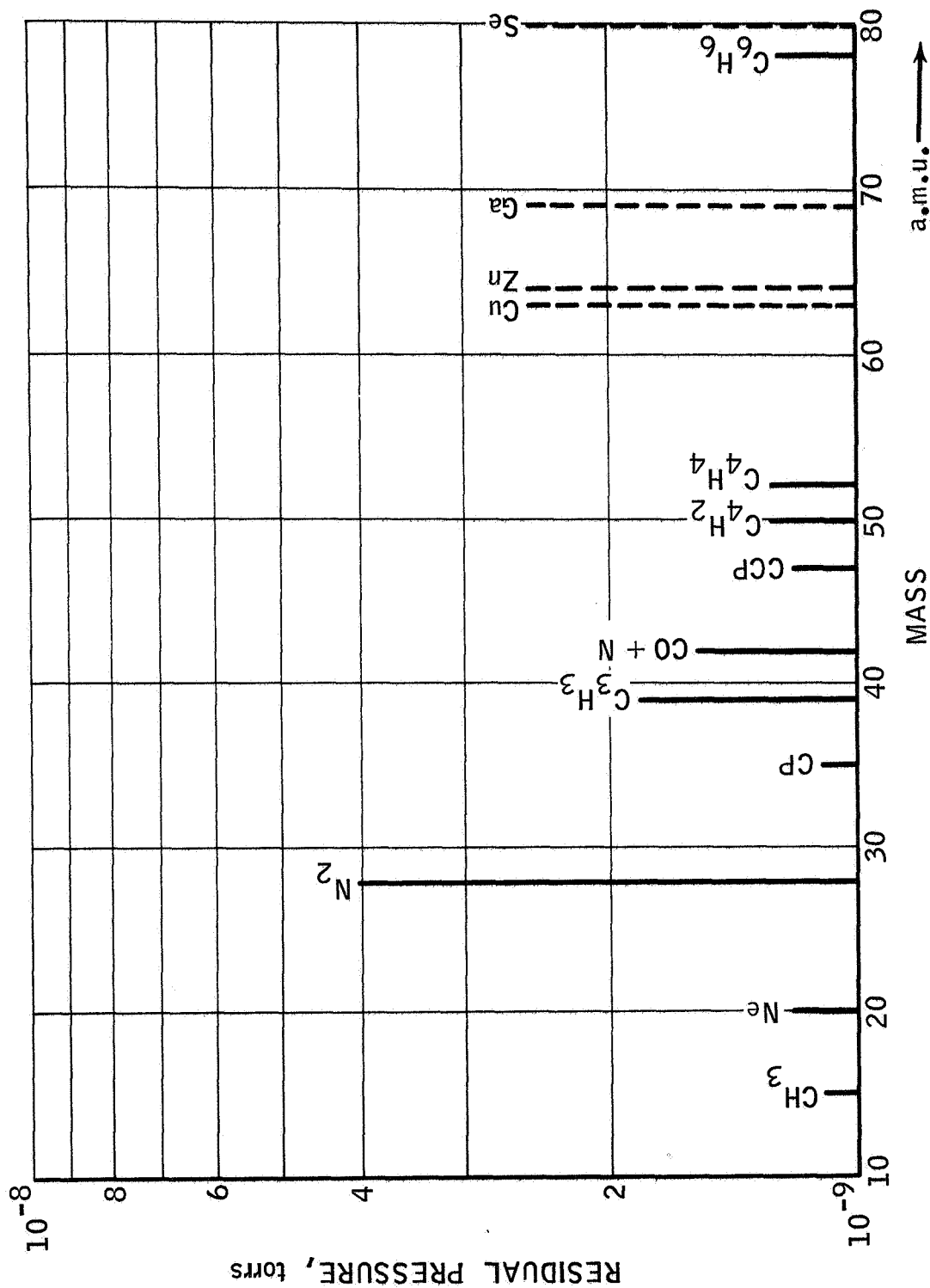


Figure 5  
MASS SPECTROGRAPHIC ANALYSIS OF RESIDUALS

applied between the thoriated tungsten filament and the wall of the Se crucible. The diode current was adjusted between 200 to 300 millamps. This collision approach in breaking the atomic clusters of the chalcogene polymers<sup>(1)</sup> has shown the evolving vapor to be essentially monomeric, Figure 6. The actual discrepancy observable between the isotope amplitude of mass 78 and 80 of Se, comes from the residual pressure of C<sub>6</sub>H<sub>6</sub> of benzene shown in Figure 5.

The output of Pt Rh and ion-constantan thermocouples attached to sources and substrate heater controlled the respective temperatures to within  $\pm 1^{\circ}\text{C}$ . A good thermal contact was assured between substrates and heater, the drop in temperature due to substrate thermal conductivity was accounted for.

#### Vapor Deposition

Thermodynamic third law method was applied in calculating total and partial pressures from,

$$-\log K_p = \frac{\Delta f_{\text{ef}} + \frac{\Delta H_{298}}{T}}{4.576}$$

where  $P = p_{\text{ZnSe}} + p_{\text{Zn}} + p_{\text{Se}}$

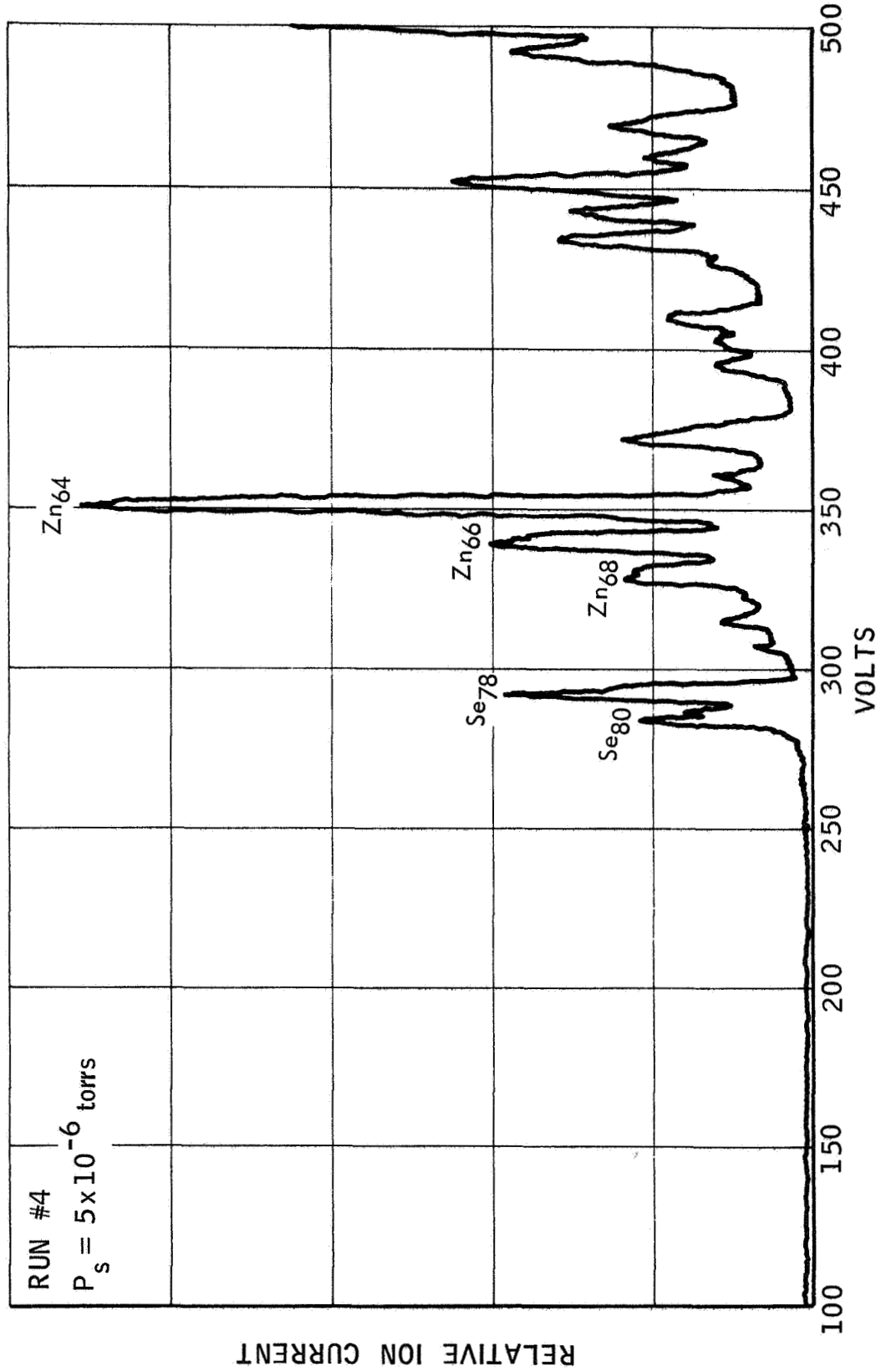
The detailed calculations are reported in Appendix II.

Since the main interest is actually directed towards ZnSe, only the results for this compound are summarized in Figure 7, representing the molecular concentration of specie i at a source temperature T, as  $n_i = f(T)$ , from the relation,

$$n_i = \frac{P_i}{(2\pi m_i kT)^{1/2}} \quad \text{cm}^{-2} \text{sec}^{-1} \quad (1)$$

It is seen that the molecular concentration from the evaporating compound is far below the values of any of the two components.

Present nucleation theories do not permit a straightforward approach in calculating condensation parameters for binary vapors. Actually a purely experimental approach was followed in evaluating the epitaxial deposition of ZnSe and ZnTe.



R-26,646

Figure 6  
 MASS SPECTROGRAPHY OF COEVAPORATED Zn + Se  
 CONCENTRIC TMC SOURCES. THERMAL IONIZER.

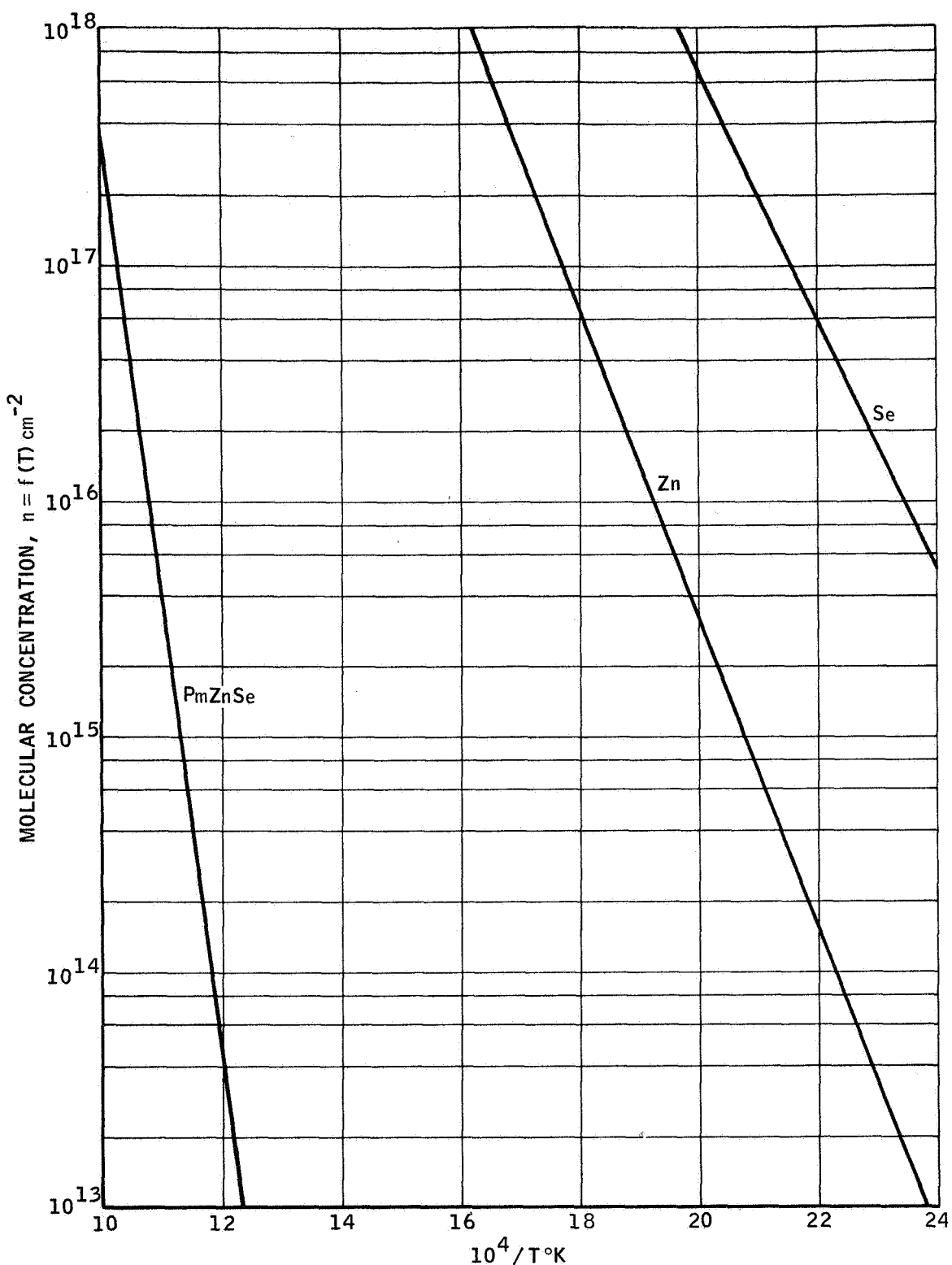


Figure 7  
 EQUILIBRIUM CONCENTRATION

R-26,939

The main object of this phase of the work was first to assess the role of the substrate temperature vs. the molecular concentration (eq. 1) on the film's stoichiometry. The second step was to investigate the interdependence between substrate temperature, molecular concentration, and angle of vapor incidence on the film crystallization.

During evaporation of any II-VI compounds, dissociation occurs and the compound reconstitutes itself during condensation by chemical association between elements. It is well established that this occurs even when the condensation temperature is well above the critical condensation temperature of the elements, irrespective of the vapor concentrations.

The current procedure adopted in this work was to keep one source at a constant pressure, while the other was used as the variable, for each new setting of substrate temperature.

The condensation rate of the ZnSe compound is shown in Figure 8, on which stoichiometric range has been plotted. Each film was evaluated for composition by X-ray fluoroscopy; the results of these measurements are shown in Figure 9. The deviations from stoichiometry is shown to increase rapidly as a function of vapor composition. The large ratio Se/Zn accounts for several conditions, first, the lower critical condensation temperature for Se compared to Zn. Secondly, it was observed that a higher Se content in the impinging vapors favors one particular crystalline structure. The density of trapping centers in II-VI compounds is structure sensitive and was found to increase with increasing contribution from mixed crystalline phases.

It can be seen from these measurements that stoichiometry occurs only in a fairly narrow range of vapor concentrations for any condensation temperature experimented with.

#### Crystalline Structure

Both ZnSe and ZnTe are known to have polymorphic structures, i.e., they both can occur in cubic and hexagonal phases.<sup>(12)(13)</sup> As a guide to structure identification, the position of the main planes of a ZnSe crystal are indicated as a function of the refracting angle in Figure 10. In these figures the respective reflection intensities are shown for both cubic and hexagonal planes.

Along with the crystal plane identification, the procedure involved an evaluation of the degree of crystallization of the films correlated with the processing parameters.

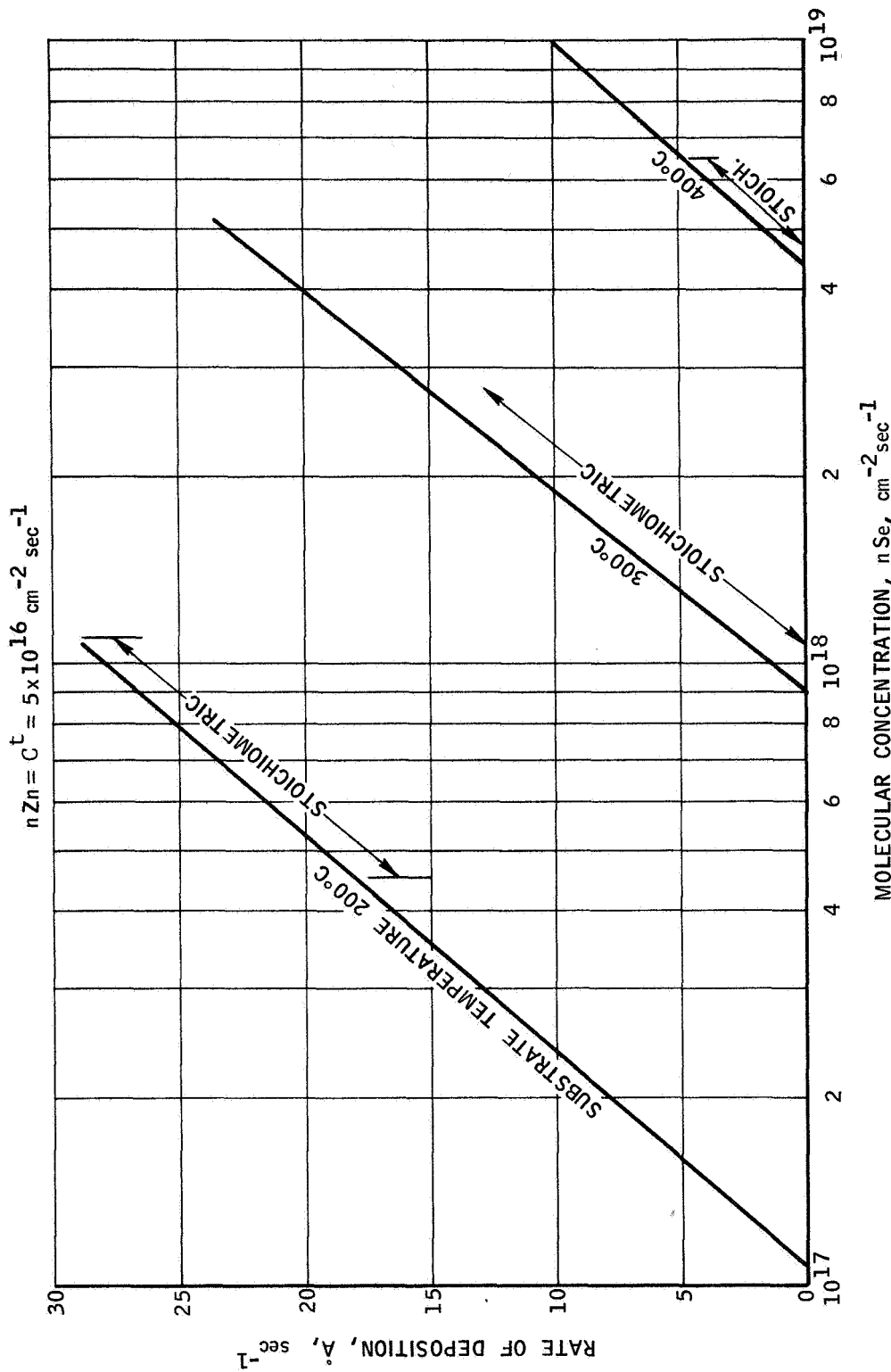


Figure 8  
 GROWTH OF ZnSe LAYER FUNCTION OF MOLECULAR FLUXES

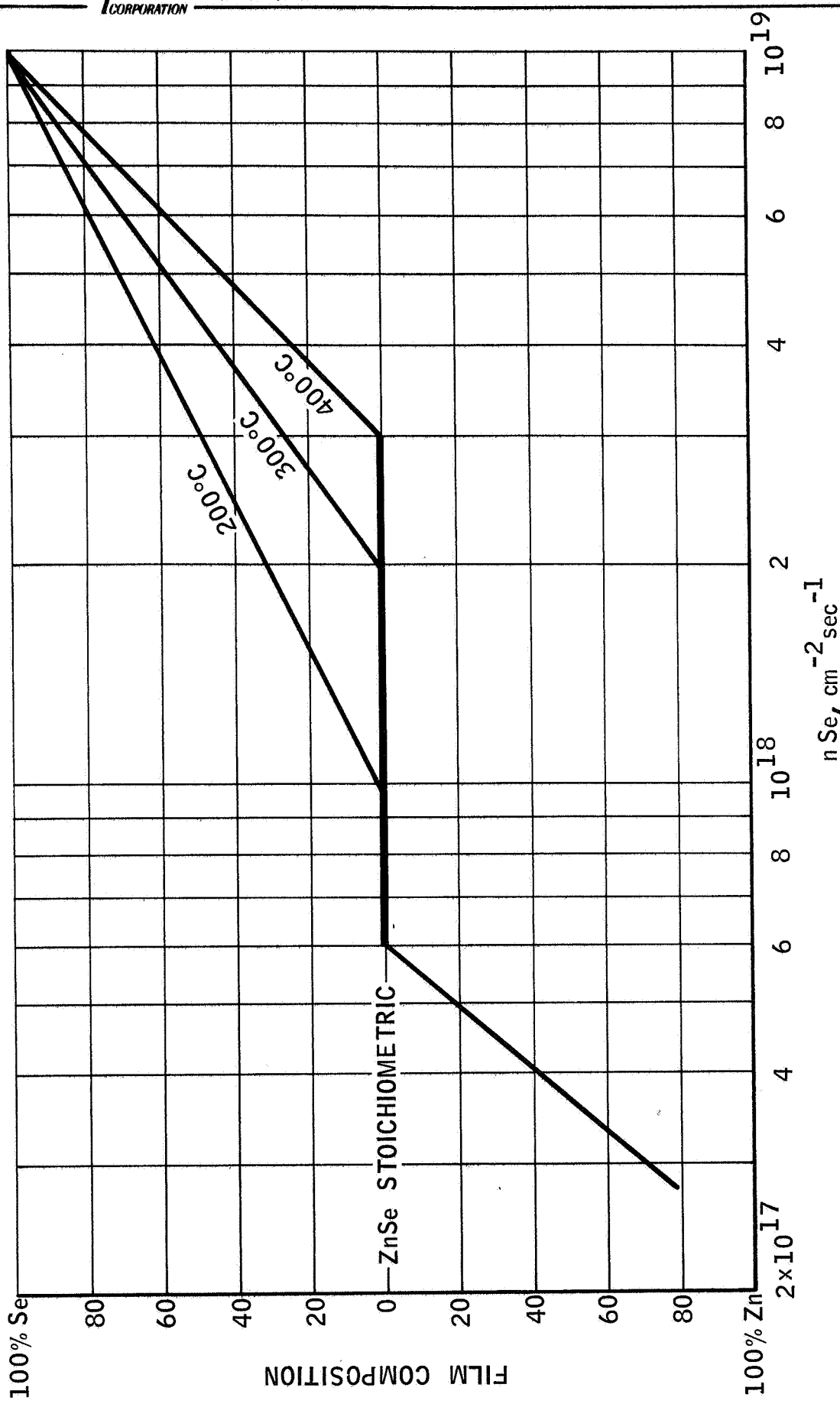


Figure 9  
 FILM COMPOSITION vs. Se FLUX AT Zn FLUX CONSTANT

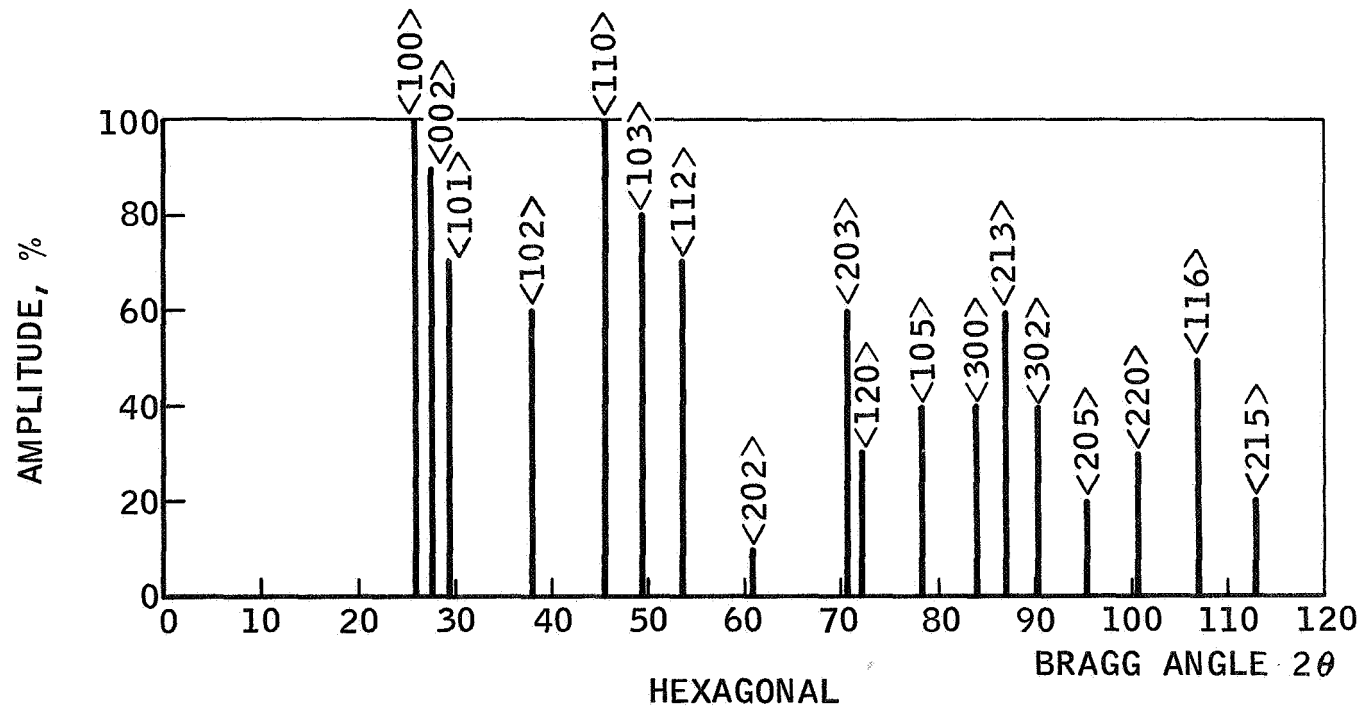
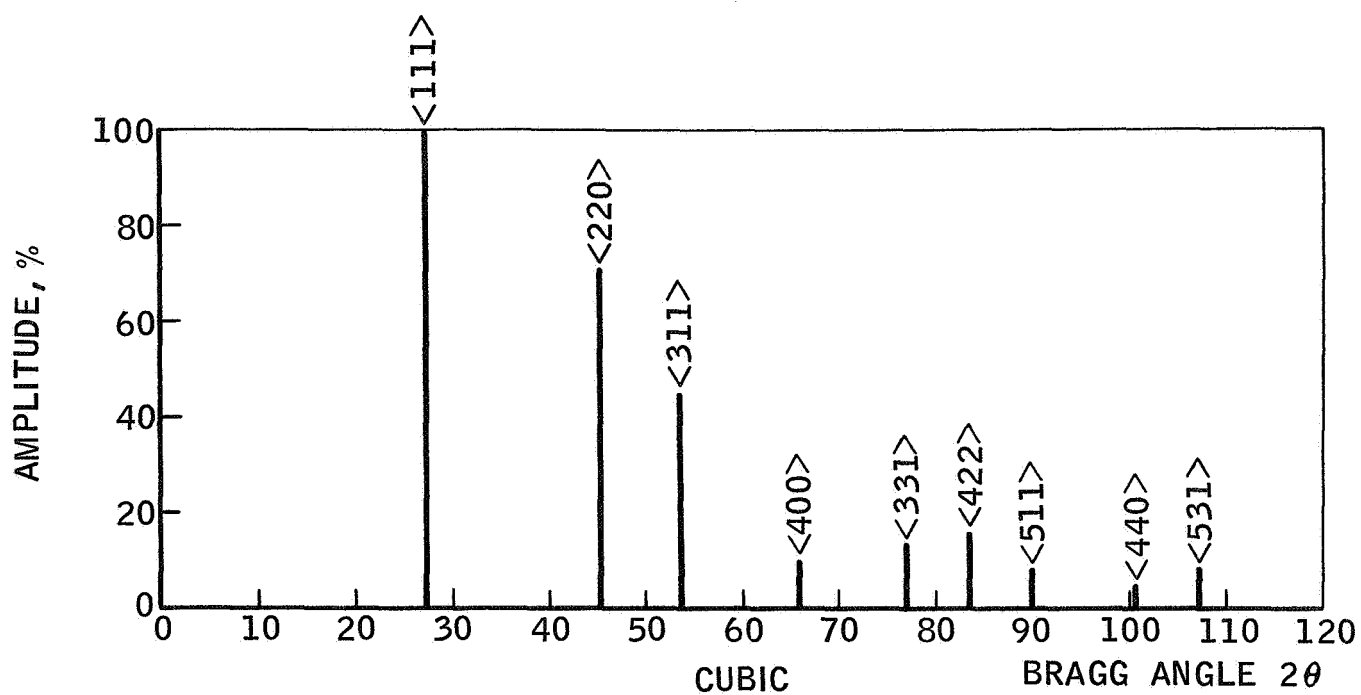


Figure 10  
 ZINC SELENIDE DIFFRACTION PATTERNS

Plane spacings in Debye Scherrer photographs were calculated by Straumanis' method: in these, or in diffractometer recordings, the CuK $\alpha$  wavelength<sup>(14)</sup> was used throughout. In back reflections, calculation of position and indices of Laue spots was made from Kedesy method.<sup>(15)</sup>

Attempts to use Scherrer's equation, for crystallite size determination, from,<sup>(16)</sup>

$$D = \frac{0.9\lambda}{\beta \cos \theta}$$

( $\theta$  Bragg angle;  $\beta$  half breadth;  $\lambda$  = CuK  $\alpha$ )

proved to be too cumbersome to manipulate in most cases. A simpler, though qualitative method<sup>(17)</sup> was used instead.

On back reflection Laue photographs, a parameter R defines the degree of crystallization; it is given the value 0 for patterns showing only diffused rings; a value of 25 is assigned to R for mixed rings and spots pattern in which the ring aspect predominates; 50 for R indicates that spots and rings have identical intensities; 75 is assigned to mixed patterns where the spots predominate; finally R is equal 100 for spots pattern only.

The slope of the straight line describing  $R = f(T)$  was obtained from least square method, from,

$$\frac{Y_R}{X_T} = \frac{n \sum XY - \sum X \sum Y}{n \sum X^2 - (\sum X)^2}$$

with n, the number of experimental points.

A graphical representation of this function is given in Figure 11 in a) for ZnSe, and in b) for ZnTe.

Back reflection Laue spots from perfect crystals are sharp, while arcing of the spot reveals that the deposit contains nuclei rotated about the normal to the specimen plane. Fine rings indicate a well defined structure but made up of small crystallites. The Laue photographs shown in Figure 12 to 15 illustrate the various steps in the process for ZnSe and in Figure 16 and 17 for ZnTe.

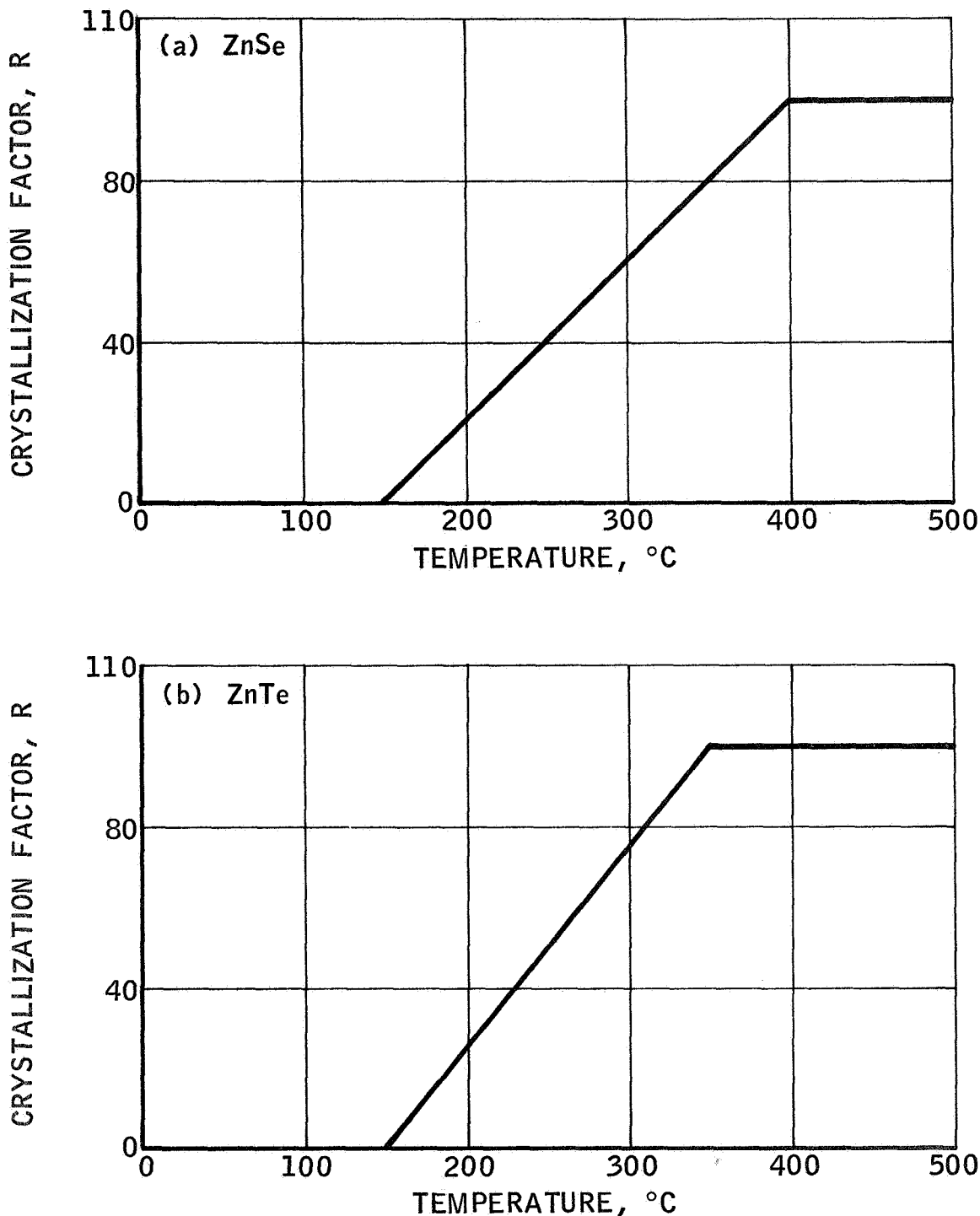
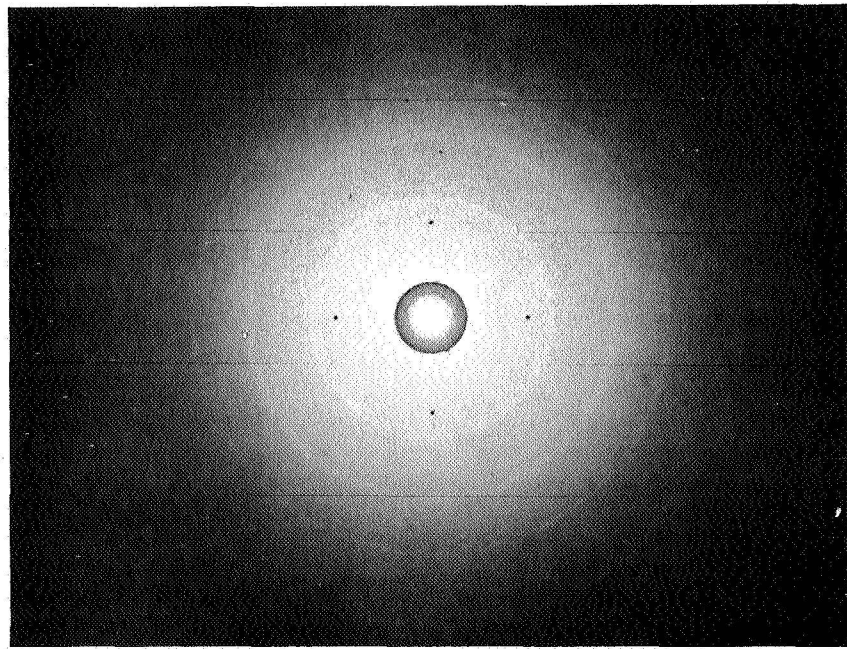
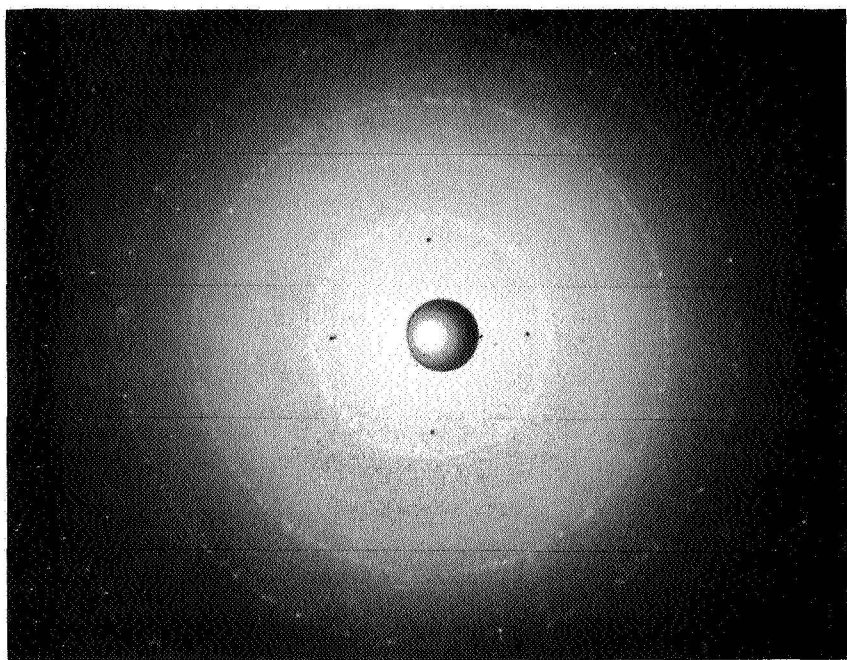


Figure 11  
EPITAXIAL GROWTH ON <0001> SAPPHIRE



(a)

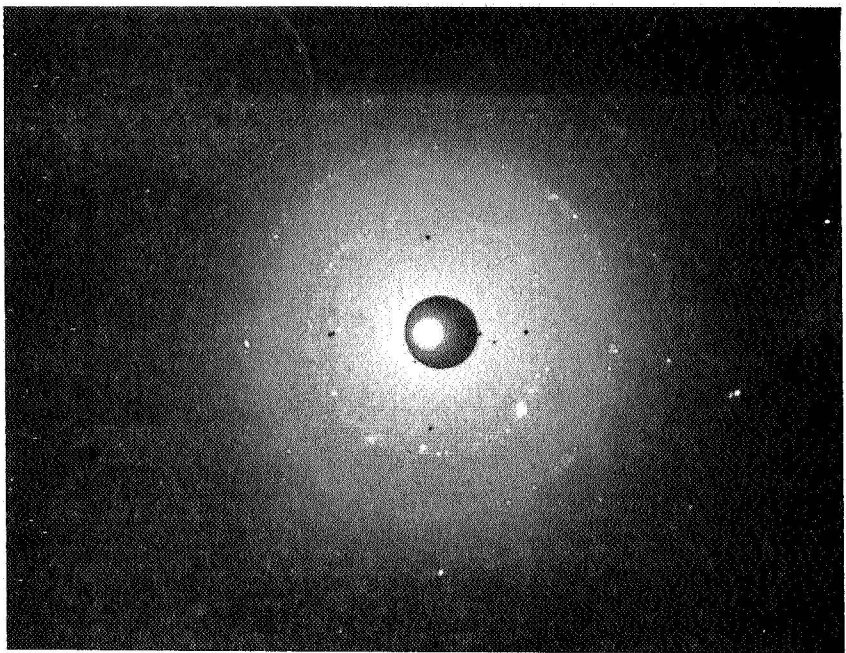
$R = 0$



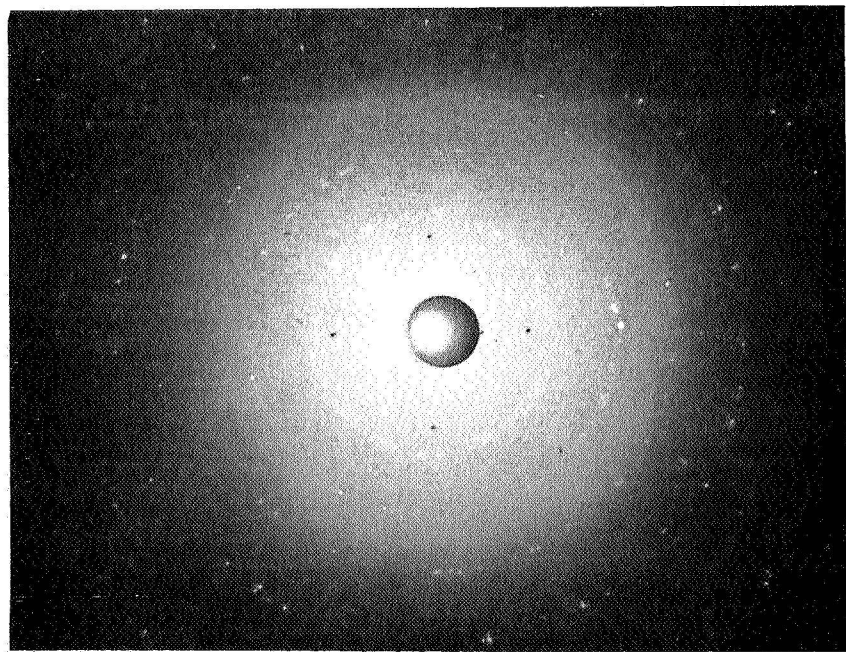
(b)

$R = 40$

Figure 12  
EPITAXIAL ZnSe LAUE PATTERNS

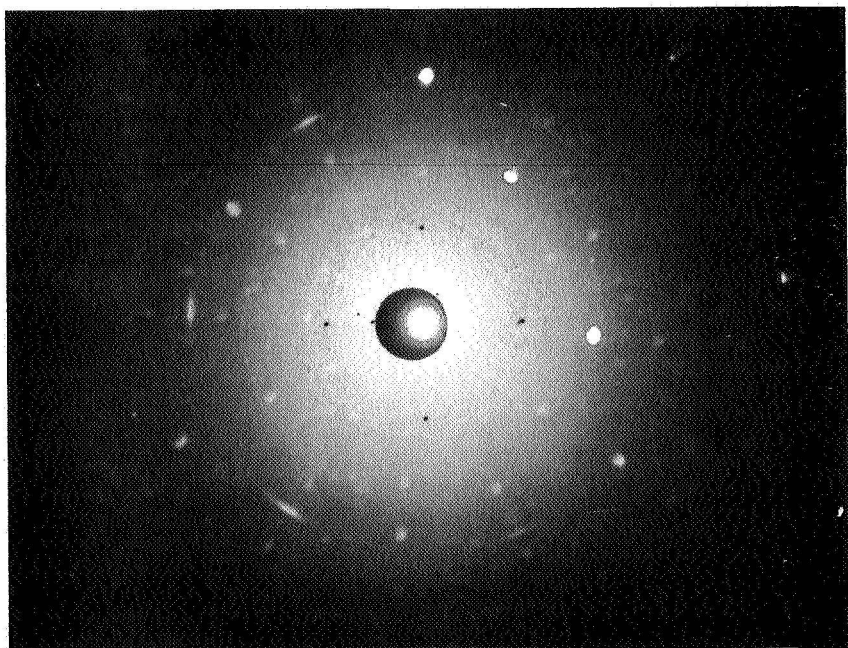


(d)                     $R = 75$

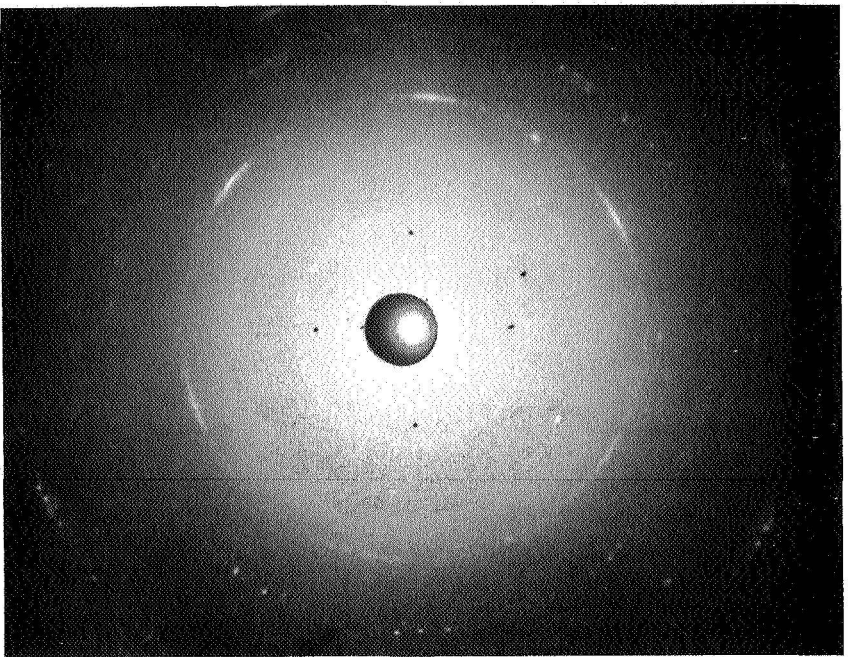


(c)                     $R = 75$

Figure 13  
EPITAXIAL ZnSe LAUE PATTERNS

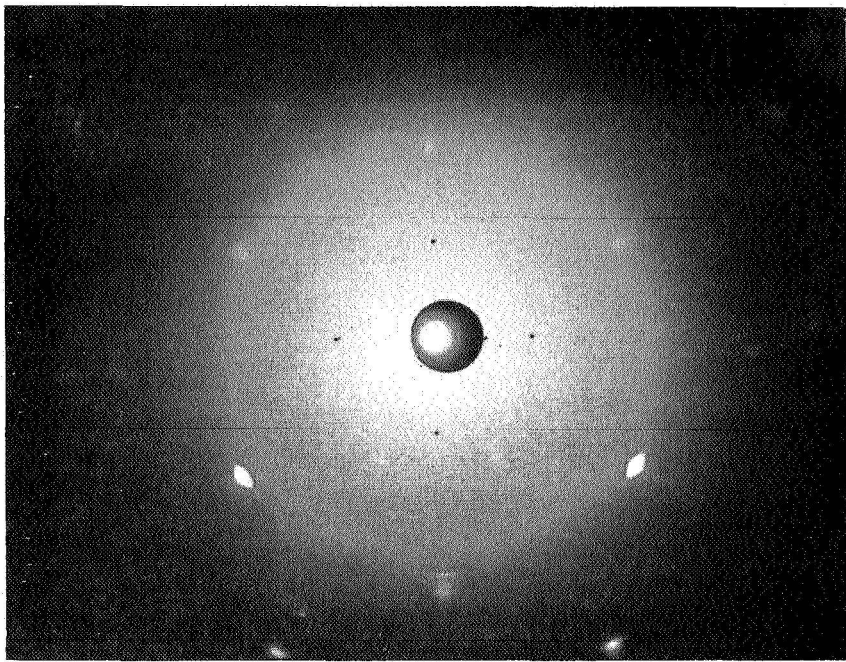


(e) THIN FILM

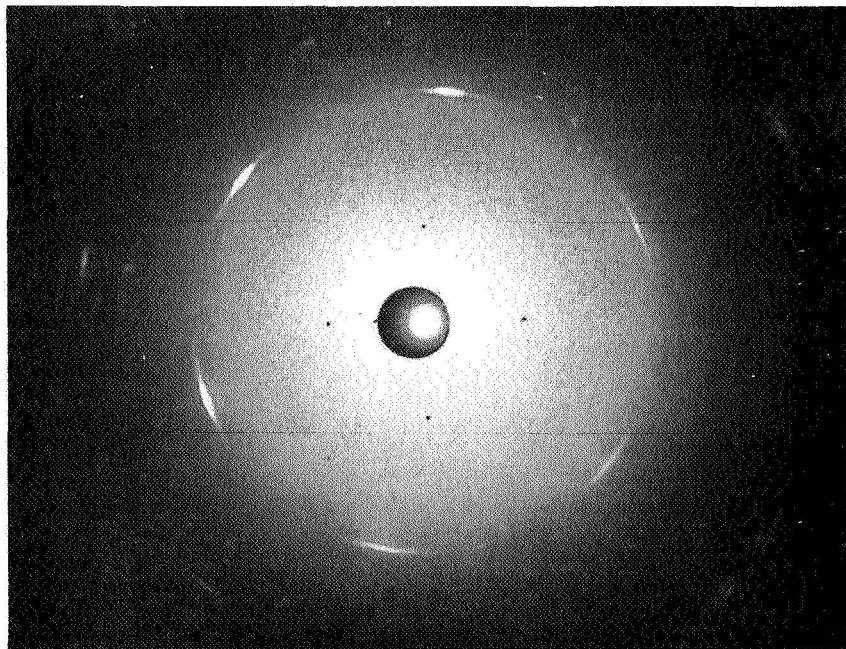


(f)  $R = 50$

Figure 14  
EPITAXIAL ZnSe LAUE PATTERNS

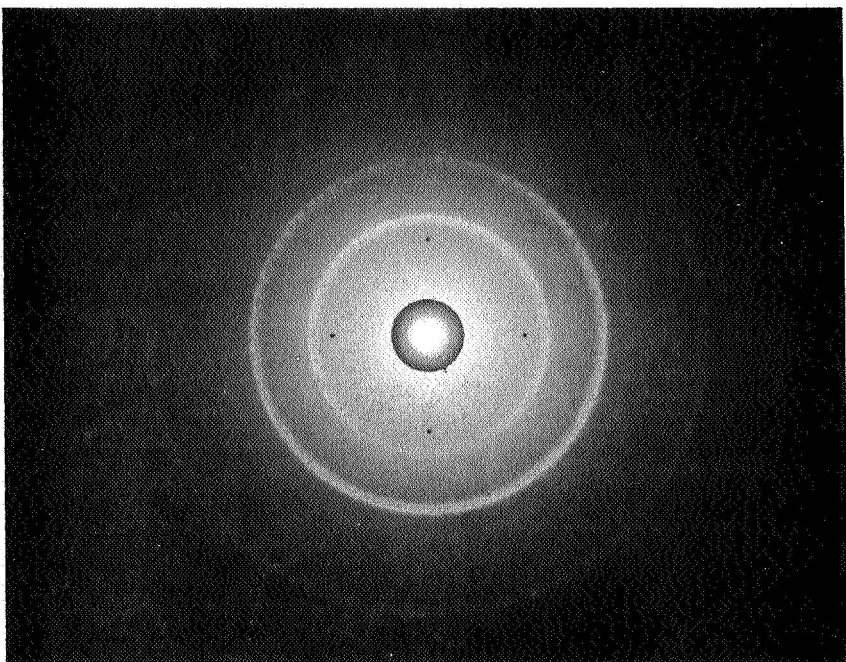


(h)  $R = 100$

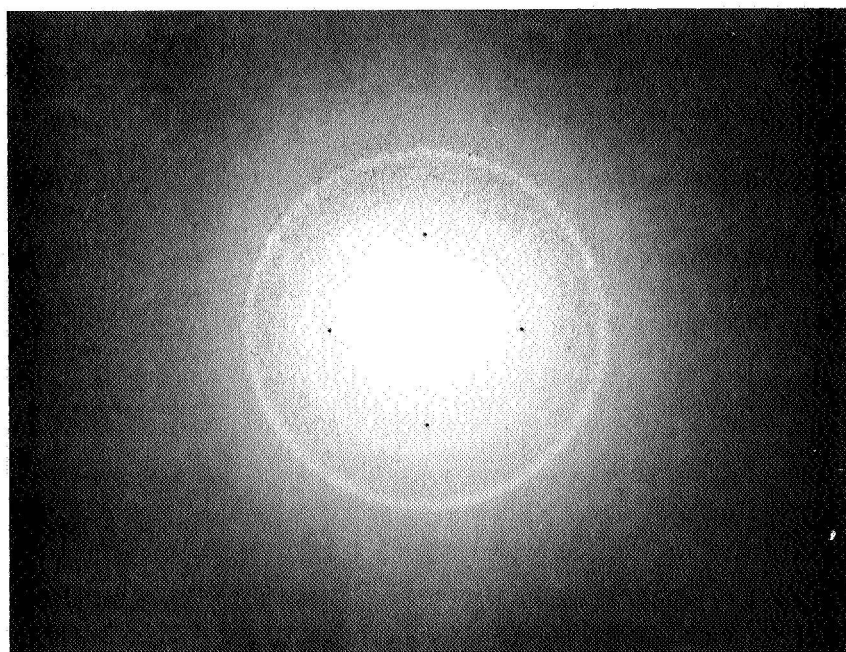


(g)  $R = 90$

Figure 15  
EPITAXIAL ZnSe LAUE PATTERNS

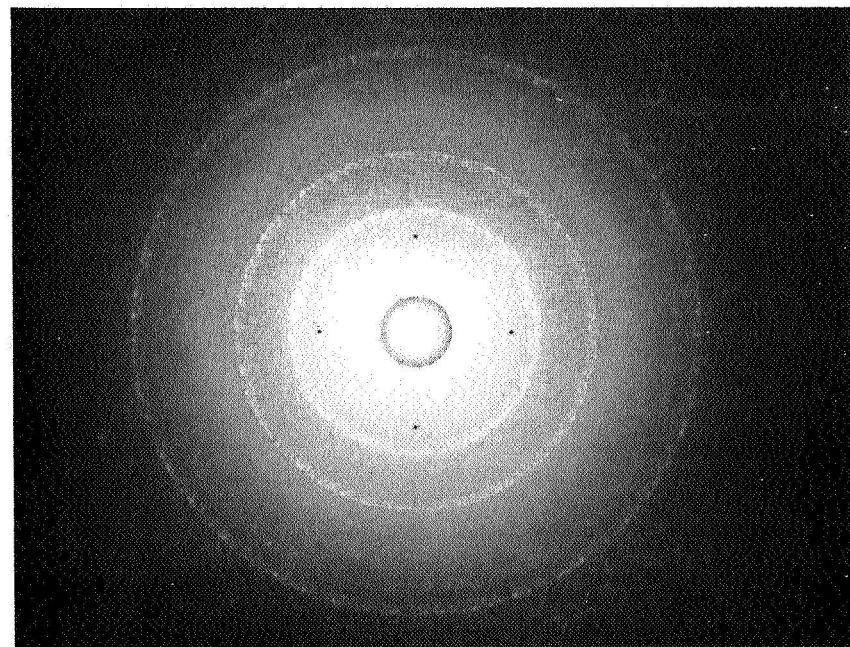


(b)  $R = 20$



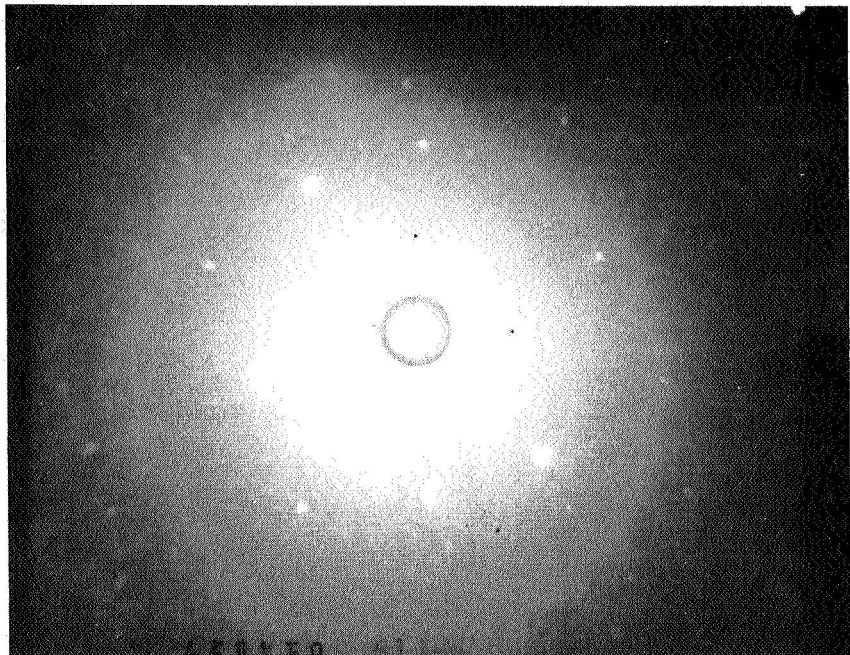
(a)  $R = 0$

Figure 16  
EPITAXIAL ZnTe LAUE PATTERNS



(c)

R = 75



(d)

$T_c = 400^{\circ}\text{C}$  R = 100

EPITAXIAL ZnTe LAUE PATTERNS

Figure 17

Figure 12 a) corresponds to a substrate temperature of 150°C and 250°C for b).

Figure 13 c) and d) were obtained for an identical substrate temperature but at different incident nZn, they show clearly varying contributions of the hexagonal phase.

Figure 14 e) shows the reflection produced by the <0001> sapphire with a film of ZnSe of thickness around 1500 Å.

f) shows an increased organization in the nuclei towards a cubic structure, although the hexagonal contribution is still significant.

Figure 15 g) shows only the main plane of the cubic phase with the three fold symmetry of <111> ZnSe well defined; although monocrystalline structure is not attained a clear tendency to three dimensional organization is visible.

h) with the slightly elongated spots indicates a near perfect epitaxy a substrate temperature of 400°C. This film contains only the cubic phase.

The following conclusions summarize the observations made. Increased concentration in the impinging vapor favors the formation of the hexagonal phase, as does condensation at low substrate temperature. A pure hexagonal phase could not be obtained within the angle of incidence achieved in this work. Grazing incidence to produce the hexagonal modification<sup>(18)</sup> was not verified in this work. The hexagonal phase has been found to be more sensitive to composition of the impinging vapors. Excess Se assists in forming a pure cubic phase, which is the only structural phase found in the films at temperatures above 400°C.

On etched sapphire substrates cut in the basal plane, ZnSe films, well adherent, have been grown up to 0.040" thickness. Similar procedure has been applied to ZnTe, whose function R is shown in Figure 11 b). The influence of substrate temperature on crystallization is shown in Figure 16 and 17. The perfect structure of the epitaxial film on sapphire shown in Figure 17 d) has been obtained at a condensation temperature above the value at which epitaxy sets, presently at 425°C.

### Electroluminescent Devices

#### a) Constraints in II-VI Devices

As stated earlier, amphotermism is not achievable in large band gap materials at least to an extent where comparable conductivities for both p and n type of carriers are obtained. The availability of radiative centers will therefore be proportional to the lowest of the two concentrations.

All desirable II-VI compounds are predominantly n type, except for ZnTe, the only p type material in the series which however has a lower conductivity and is a poor phosphor.

Dissimilarities in band gaps, in lattice spacings, in electronegativities, in solubility of dopants, in thermal coefficients of expansion have prevented the formation of abrupt homojunctions, by alloying ZnTe with another II-VI compound. ZnTe heterojunctions formed with CdS<sup>(9)(19)</sup> or with ZnSe<sup>(20)(21)</sup>, still has most of these shortcomings and radiates only in the yellow part of the spectrum. This alloying has not been successfully achieved in film form, during the course of this work.

The reduction of ohmic losses requires both a high conductivity and very thin p and n regions. The former requirements is hardly achievable when deep levels are introduced in the band gap by doping impurities<sup>(24)</sup>. Only at very high concentration can impurities bands merge with the main band and improve the efficiency at high currents; this however lowers the junction efficiency at low exciting voltage. Ultimately the maximum conductivity will be limited by solubility and segregation coefficients of doping impurities.

Until better interfacing between p and n, II-VI compounds can be secured with still unknown methods of exploiting defects chemistry these heterojunctions will remain inefficient devices.

#### b) Heterojunctions Produced

Two different types of heterojunctions were investigated during this work, one based on a pin structure, the other by using I-VI compound, or a III-V compound as the p type region.

#### Pin Structure

The first type of junction investigated had a co-planar configuration with electrodes of indium and platinum side by side onto a film of gallium doped ZnSe. A similar approach has already been discussed<sup>(25)</sup> that relies upon a potential barrier created by a high work function metal in contact

with ZnSe viz ZnSe-Pt. The other electrode material has a low work function which results in an ohmic contact with the semiconductor.

The height of the potential barrier,  $\Phi$ , through which the charge carriers gain their kinetic energy is expressed by<sup>(25)</sup>,

$$qV_D = \Phi = \phi_m - \phi_s \quad (1)$$

with:  $V_D$  the diffusion potential;  $q$  the elementary charge;  $\phi_m$  the metal work function;  $\phi_s$  the semiconductor work function,  $\phi_s \approx X^m E_F$ , where  $X = \Phi - E_g = \phi_s - E_F$  with  $X$ ,  $E_g$  and  $E_F$  respectively the semiconductor electron affinity, its band gap and Fermi level.

The surface state influences profoundly the work functions of both metal and semiconductor, as a result, the potential barrier is seldom calculable from the work function above.

The characteristics of such junction are accessible through barrier capacitance measurements, from derivation of Poisson's equation:

$$\frac{d^2\psi}{dx^2} = \frac{qNd}{\epsilon\epsilon_0} \quad (2)$$

with:  $\psi = (V_D + V)$  at  $x = d$ ;  $d$  the barrier thickness;  $V$  the applied voltage;  $Nd$  the donor density;  $\epsilon$  the dielectric constant of ZnSe;  $\epsilon_0$  free space permitivity we have

$$(V_D + V) = \frac{qNd}{2\epsilon\epsilon_0} d^2 \quad (3)$$

Since the charge  $Q$  per unit area is

$$Q = qN_d d = \left[ 2\epsilon\epsilon_0 qNd(V_D + V) \right]^{\frac{1}{2}} \quad (4)$$

the junction capacitance follows from

$$C = \frac{dQ}{dV} = \left[ \frac{q\epsilon\epsilon_0 Nd}{2(V_D + V)} \right]^{\frac{1}{2}} \quad (5)$$

the thickness of the barrier is obtained from equation (3) as

$$d = \left[ \frac{2\epsilon\epsilon_0}{qNd} (V_D + V) \right]^{\frac{1}{2}} \quad (6)$$

Equation (4) may be written in the form,

$$\frac{d(1/C^2)}{dV} = \frac{2}{q \epsilon \epsilon_0 N_d} \quad (7)$$

from which the carrier concentration gives

$$N_d = \frac{2}{q \epsilon \epsilon_0} \frac{dV}{d(1/C^2)} \quad (8)$$

extrapolating  $1/C^2$  to zero gives the value of the diffusion potential  $V_D$ .

The current voltage relationship in such electroluminescent diode, is represented by

$$I = I_o \left( \exp^{-\frac{qV}{kT}} - 1 \right) \quad (9)$$

where the saturation current  $I_o$  is obtained from the equation

$$I_o = \left( \frac{4 \pi q m^* k^2}{h^3} \right) T^2 \exp - \frac{\phi_m - X}{kT} \quad (10)$$

with  $m^*$  the effective mass;  $k$  Boltzmann's constant,  $h$  Planck's constant;  $T$  the temperature.

The probability of generating electroluminescence by field ionization when operating the diode in the reverse direction may be calculated from<sup>(27)</sup>

$$P = \frac{qEdn}{h} \exp \left[ -\frac{\pi^2}{2qhE} \sqrt{2m^*} E_g^{3/2} \right] \quad (11)$$

with  $E$  the field strength  $E = (2V_D + V)/dn$  across the junction;  $dn$  the nearest neighbor distance  $dn = a_o \sqrt{3}/4$  with  $a_o$  the lattice constant of ZnSe  $a_o = 5.658\text{\AA}$ .

Measurements were performed with a Boonton bridge at  $1\text{Mc sec}^{-1}$  with a built in DC power supply providing the voltage  $V$ . The capacitance of a junction area approximately  $5 \times 10^{-3} \text{ cm}^2$  has been plotted as a function of voltage. Figure 18(a) introducing the constants  $\epsilon = 8.7$  for ZnSe;  $\epsilon = 8.85 \times 10^{-14} \text{ Fd cm}^{-2}$  in the function  $1/C^2 = f(V)$  yields a carrier concentration  $N_d \approx 10^{18} \text{ cm}^{-3}$  with about one order of magnitude discrepancy from

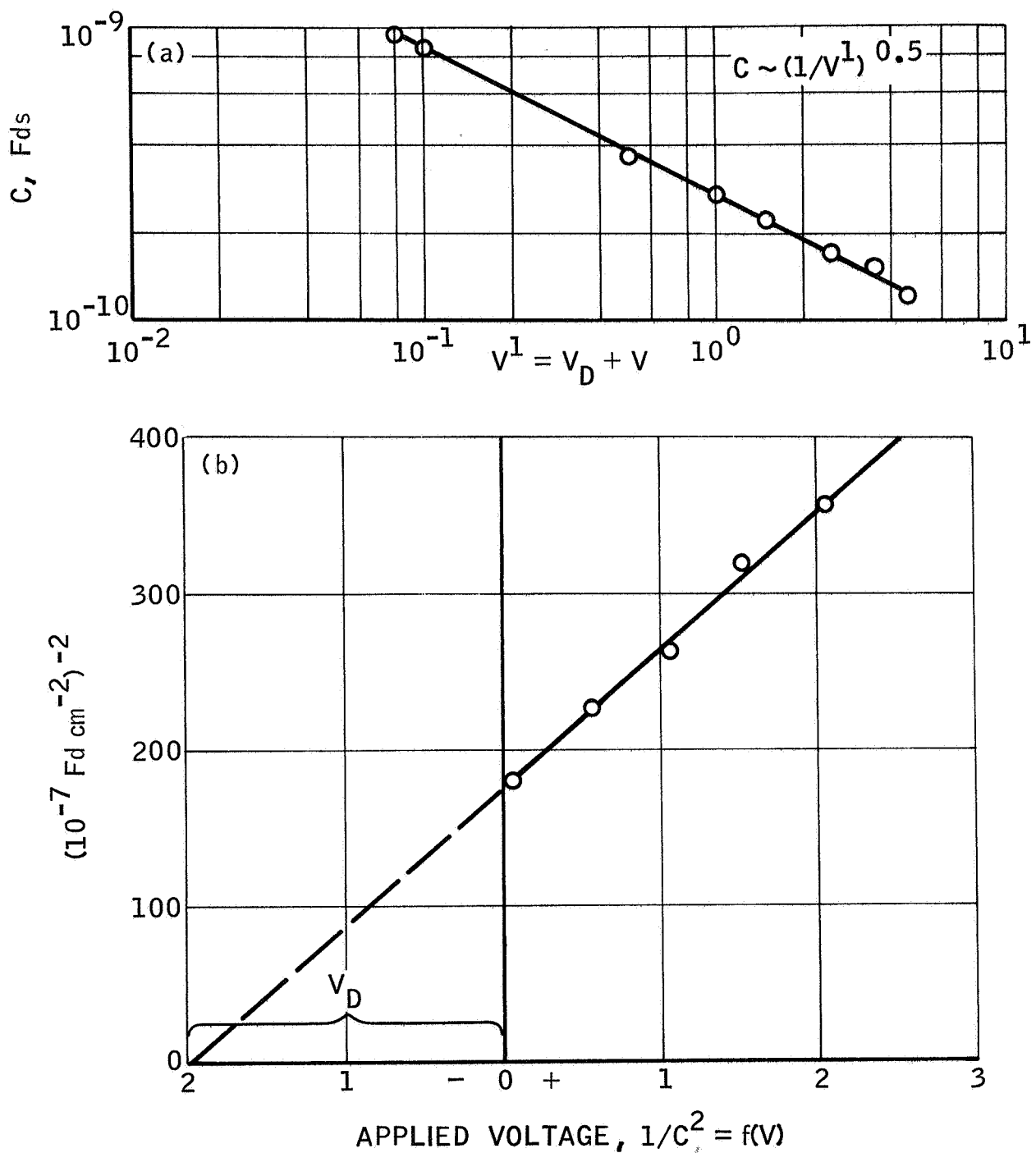


Figure 18  
 CAPACITANCE vs. VOLTAGE ACROSS JUNCTION

resistivity measurements. From extrapolation of  $1/C^2$ , Figure 18(b), a diffusion voltage of 1.98 volt is found, whereas extrapolating the function current voltage Figure 19, a value of 2.1 volts is obtained; the discrepancy between the two values is small and well within the errors due to the small junction area. With a barrier's thickness calculated from equation (6) of  $\approx 4 \times 10^{-4}$  cm the probability from equation (11) approaches unity as the voltage approaches 20 volts.

The current voltage relationship for the diodes tested is shown in Figure 19 and emission spectrum plotted at room temperature in Figure 20.

The brightness has been measured by bringing in the vicinity of the diode surface a fiber optics coupled with the photomultiplier of a Gamma photometer. The brightness has been plotted as a function of the diode current in Figure 21. This plot indicates a light intensity proportional to the current within the range of current investigated.

The efficiency of the electroluminescent diode was evaluated, taking into account the spectral response and the steradiancy between junction's plane and fiber optics from

$$k = \frac{BSQ \cdot 10^{17}}{1.26L} \quad (12)$$

where K represents the number of quanta emitted per second; Q the integrated quantum output in  $d\lambda$ ; L the luminosity factor of the spectrum; B the brightness in foot Lambert.

The measurements were repeated within the linear range shown in Figure 21 to give

$$\frac{qK}{i} \times 100 = \text{efficiency in percent} \quad (13)$$

with i the current in amperes.

The efficiency of the diode tested was found to vary between 0.1 to 0.05 percent, i.e.  $10^4$  or more electrons per photon. A photograph of the model is shown in Figure 22.

### III-V - II-VI Structure

This form of heterojunction is expected to provide a set of conditions more favorable for an efficient injection mechanism than existing in other models.

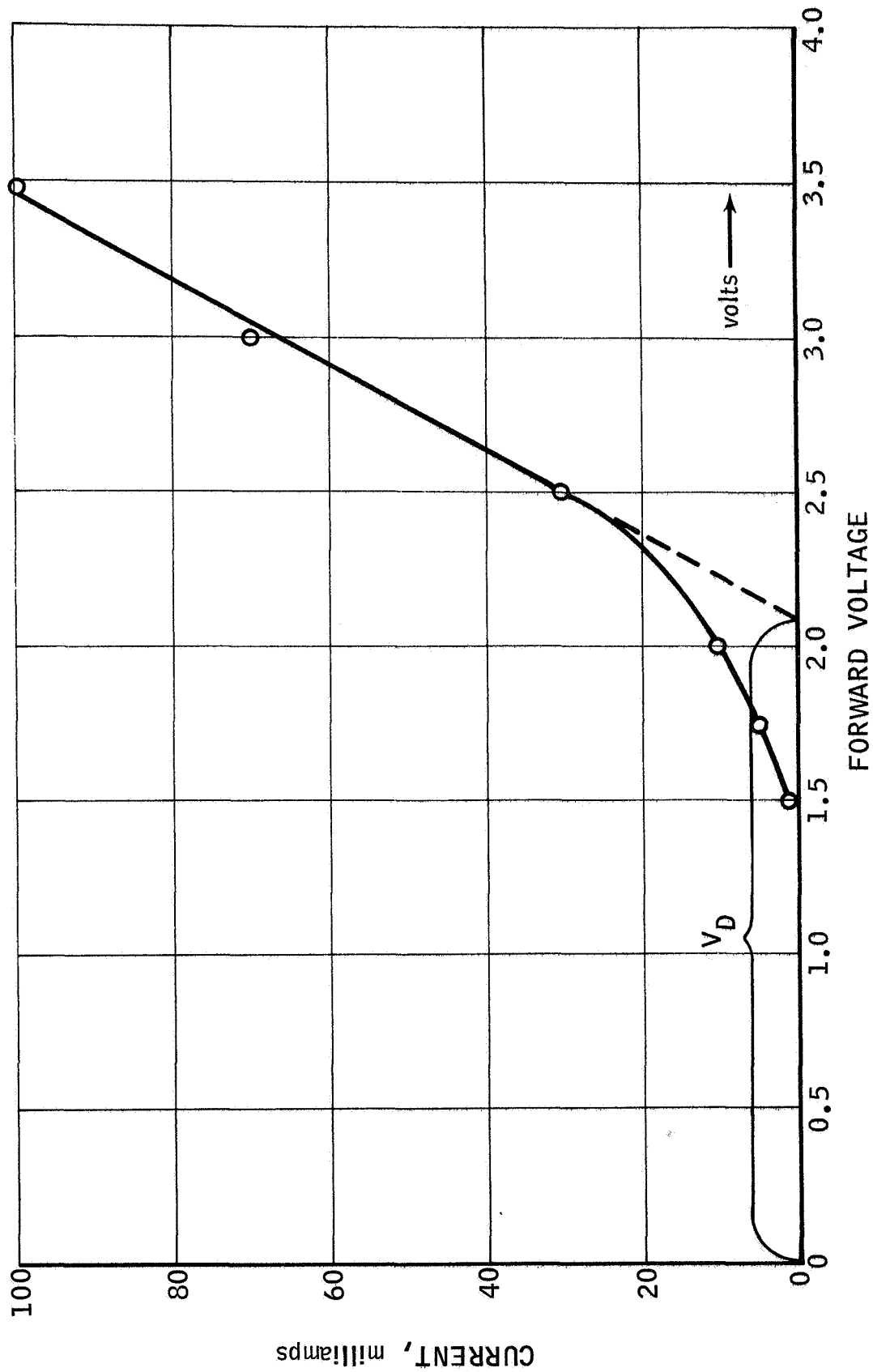


Figure 19  
pin DIODE VOLTAGE-CURRENT RELATIONSHIP

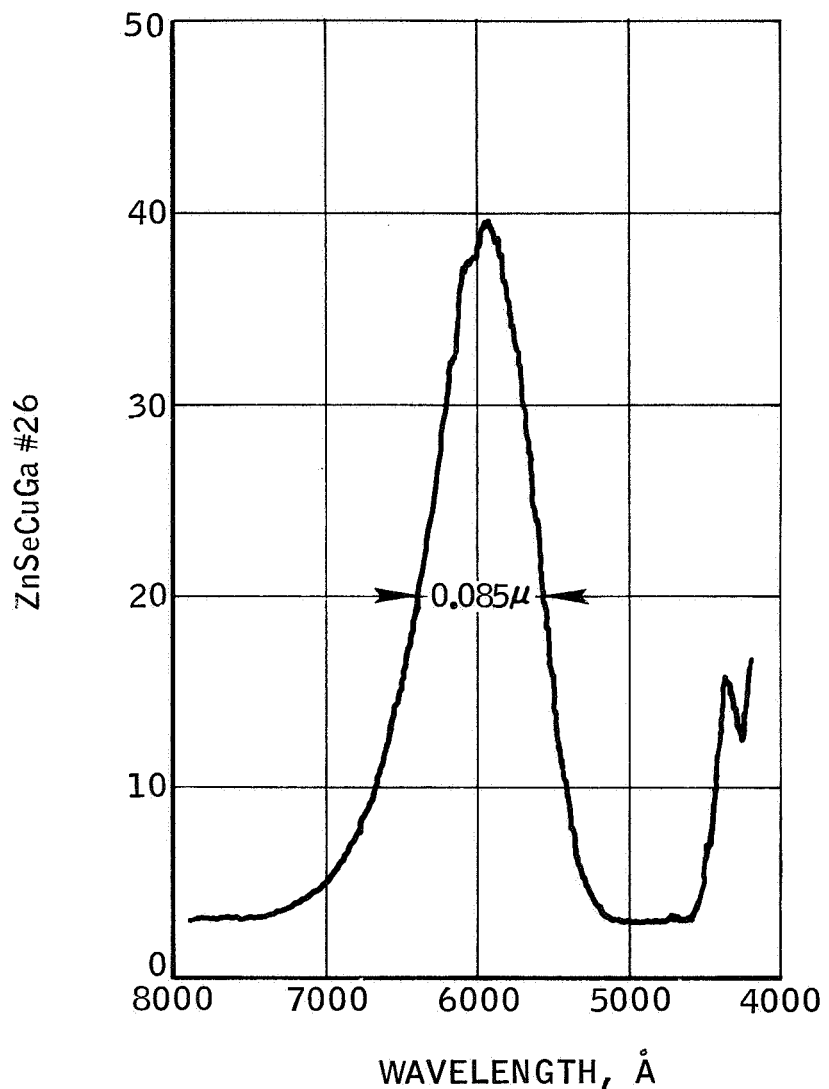


Figure 20  
pin DIODE ZnSeGa SPECTRAL EMISSION

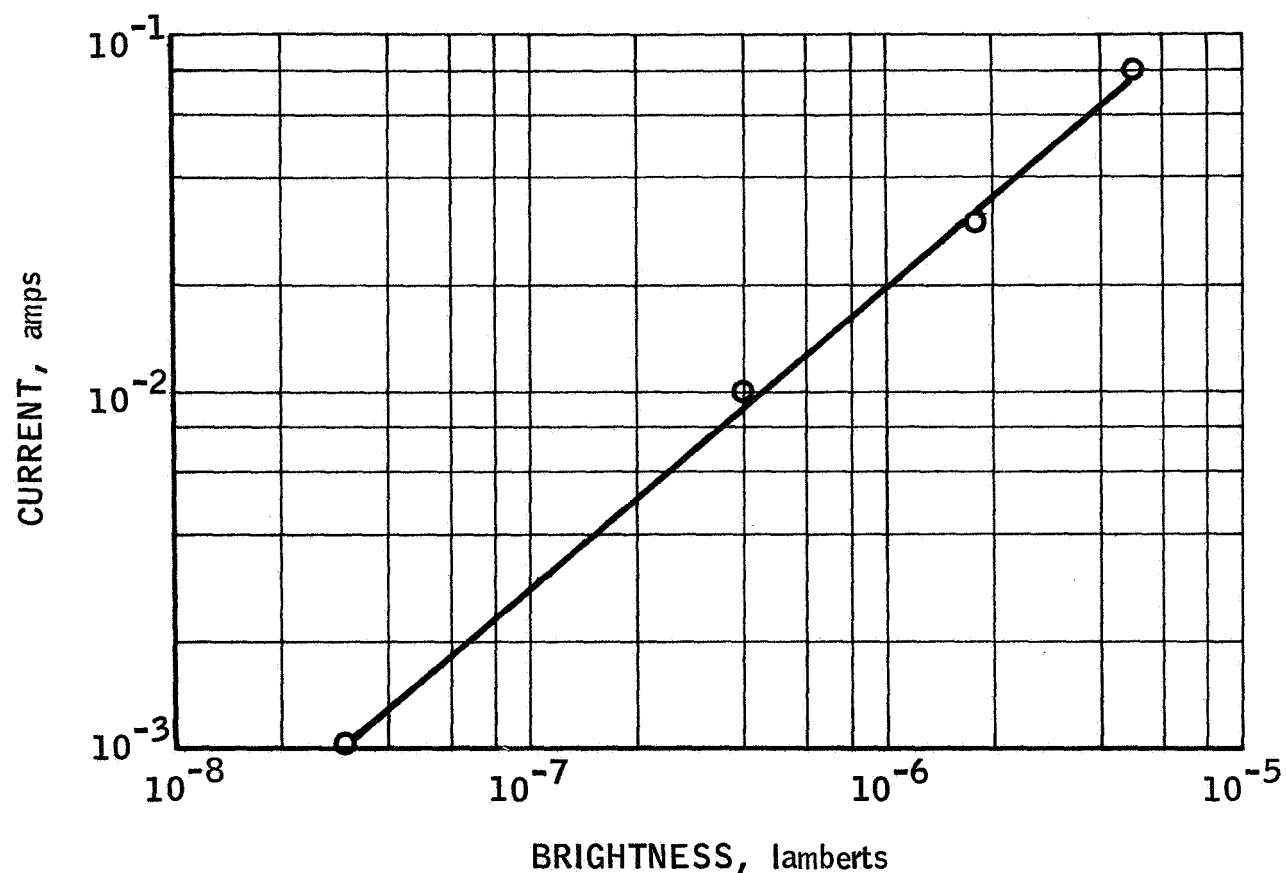


Figure 21  
CURRENT-BRIGHTNESS RELATIONSHIP

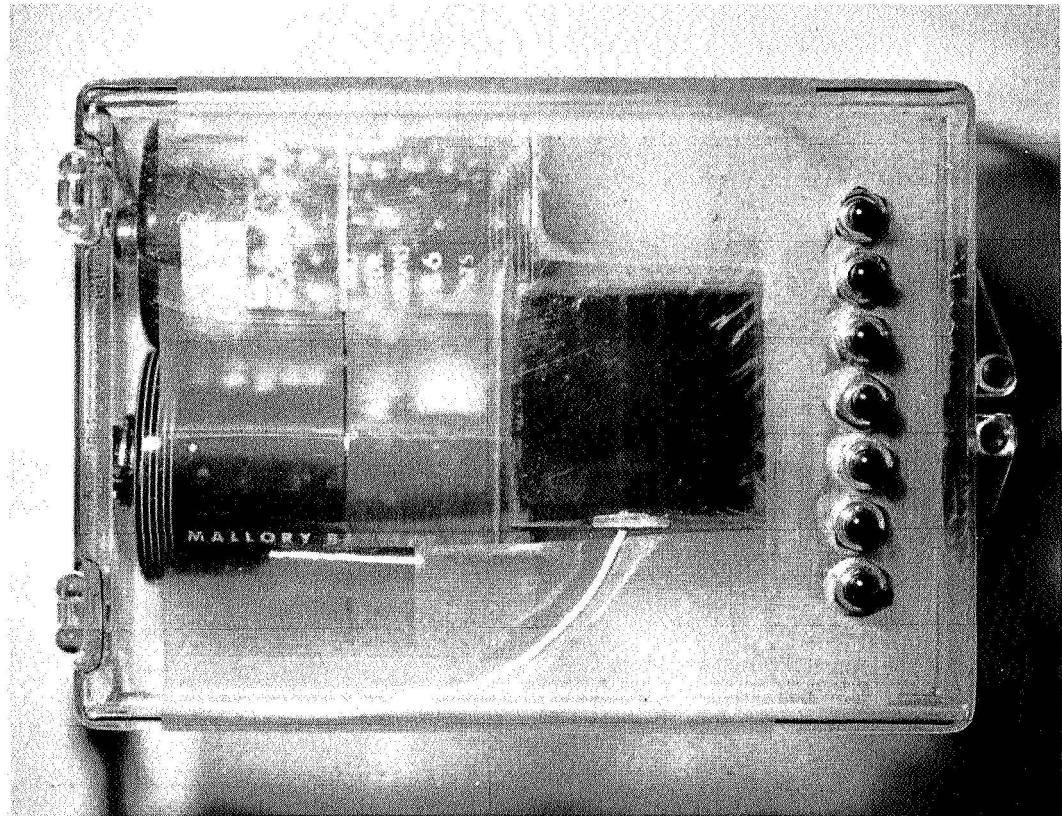


Figure 22  
ELECTROLUMINESCENT MODEL

R-26,931

Heterojunctions based on other than II-VI compounds, for example, Cu<sub>2</sub>Se-ZnSe have already been experimented with<sup>(28)</sup>.

The conductivity of 30 mhos of p type copper chalcogenide deposited upon ZnSe crystals can provide a higher holes injection rate than from ZnTe.

Furthermore near pseudo epitaxy can be expected between Cu<sub>2</sub>Se and ZnSe since both belong to the same crystalline space group with nearly identical lattice spacings. In fact the mismatch between nearest neighbor distances accounts only for 2 percent. However, a large band gap discrepancy exists between the two compounds, although Cu<sub>2</sub>Se is not precisely known and does not fit the results from<sup>(29)</sup>

$$E_g = C \frac{N_a - N_c}{Z_c + Z_a} \quad (14)$$

with N valence and Z atomic number of cation and anion with C = 43 for Eg in e.v.

The value of 0.5 - 0.7 e.v. assumed<sup>(28)</sup> on the other hand fits the difference in electronegativities.

The optical properties of Cu<sub>2</sub>Se imply a very poor external efficiency for this structure, somewhat lower than those obtained with the worst of the pin junctions tested.

In an attempt to provide a high hole injection into n type ZnSe, investigation was directed towards a structure based on the combination AlAs-ZnSe.

Aluminum arsenide is a p type semiconductor with a hole density of 10<sup>20</sup> cm<sup>-3</sup>, it has a crystal structure and nearest neighbor distances identical to ZnSe<sup>(30)</sup>. Both ZnSe and AlAs have nearly identical coefficients of expansion and hardness, the indirect band gap of 2.25 e.v. of the latter compound should provide a much better fit with ZnSe than Cu<sub>2</sub>Se does.

The bulk of the effort devoted to this approach was directed towards the epitaxy of both compounds and the formation of compatible thickness.

Little data has been published on this highly reactive compound and some difficulties have been experienced during its vacuum evaporation.

## CONCLUSIONS

During the course of this work significant progress has been achieved in reducing structural defects in evaporated chalcogenide films.

Deposition over large areas of monocrystalline films of ZnSe, by epitaxy over Sapphire substrates have been successfully completed.

Doping the host crystal by coevaporated elements has yielded conductivity between 5 to 10 mhos with mobility at room temperature greater than  $300 \text{ cm}^2 \text{ volt}^{-1} \text{ sec}^{-1}$ .

The formation of rectifying barriers from pin structures has resulted in devices operable at low voltage with an efficiency between 0.1 to 0.05 percent.

Work on a new form of p-n junction has been initiated during this period. Although the preliminary results have not been presented in this report, the approach seems very promising for a greater efficiency in carrier injection electroluminescence.

In view of these results, it is believed that the heterojunction approach between Aluminum Arsenide and Zinc Selenide will lead to a much higher yield at a lower driving power. This approach should be pursued in the next development step.

### EVAPORATING SOURCES CONFIGURATION

Defects caused by vacancies which are inherent in chalcogenides may originate from different causes: first, during production of the compound, the chalcogene may assume a polymeric form, inactive in the mass action equilibrium and the higher molecular state which prevents diffusion in the lattice; second, the crystallizing compound, even when stoichiometrically perfect, may still assume more than one steric coupling and thereby exhibit several scattering modes; the ability to form neutral pairs increases with the amount of ionic bonding in the crystal.

In order to prevent the large concentration of Zn vacancies that would result from the dissociation of ZnTe during evaporation of the compound, a new type of evaporating source has been designed to evaporate the individual elements simultaneously and satisfy stoichiometry and mass action laws during the gaseous phase. This source must not only provide separate control over the equilibrium constant of each element but also obtain their equal distribution on the substrate.

The rate of effusion, from kinetic theory is given by

$$N_o = \frac{P_s}{(2\pi RM)^{\frac{1}{2}}}$$

and the number of emitted molecules landing on the substrate is

$$N = N_o \exp h/\lambda$$

where,  $P_s$  is the vapor pressure at the temperature T obtained from Gibbs' law; with M, the molecular weight, and R, the gas constant per mole, h the distance substrate-source and  $\lambda$ , the mean free path.

$$\lambda = \left( \frac{0.707K}{\pi \delta^2} \right) \left( \frac{T}{P_s} \right)$$

with k, Boltzmann's constant and  $\delta$ , the diameter of evaporating atoms or molecules,

$$\delta = 1.32 \times 10^{-8} \left( \frac{M}{\rho} \right)^{1/3}$$

In what follows assumption is made that  $\lambda \geq h$ .

The distribution along an axis,  $x$ , originating from a point directly above the source will vary according to the source configuration, hence, for a point source

$$N_p = \left( \frac{N_o}{2\pi h^2} \right) \left[ 1 + \frac{x^2}{h^2} \right]^{-\frac{3}{2}} \quad \text{point source}$$

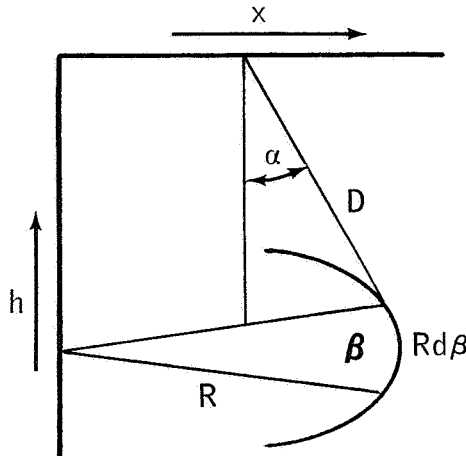
and

$$N_s = \left( \frac{N_o}{\pi h^2} \right) \left[ 1 + \left( \frac{x}{h} \right)^2 \right]^{-2} \quad \text{surface source}$$

In order to secure the same concentration of Zn and Te at any point  $x$ , the two sources must have exactly the same origin, which obviously precludes the use of surface source which can only be used side by side.

To satisfy concentration and thickness uniformities over large  $x$  values, the evaporator conceived for this task consists of two circular and concentric sources. They are individually heated by radiation. See figures, 23, 24 and 25.

With this geometry for the source, which presents a common and circular orifice of evaporation, the contribution to the coating at a point  $x$ , from a length of evaporation  $RdB$  will be proportional to



$$\frac{RdB \cos\alpha}{D^2}$$

$$\text{with } \cos\alpha = \frac{h}{D}$$

$$\text{and } D = (x^2 + R^2 + h^2 - 2xR\cos\beta)^{\frac{1}{2}}$$

the coating at  $x$  can then be expressed by

$$\int_0^\pi (x^2 + R^2 + h^2 - 2xR\cos\beta)^{-\frac{3}{2}} d\beta$$

which after expansion in powers of  $\cos\beta$  and integration, gives a series whose terms can be expanded in powers of  $x$ . The variation in coating as a function of  $x$  can then be obtained in terms of  $h$  and  $R$  only.

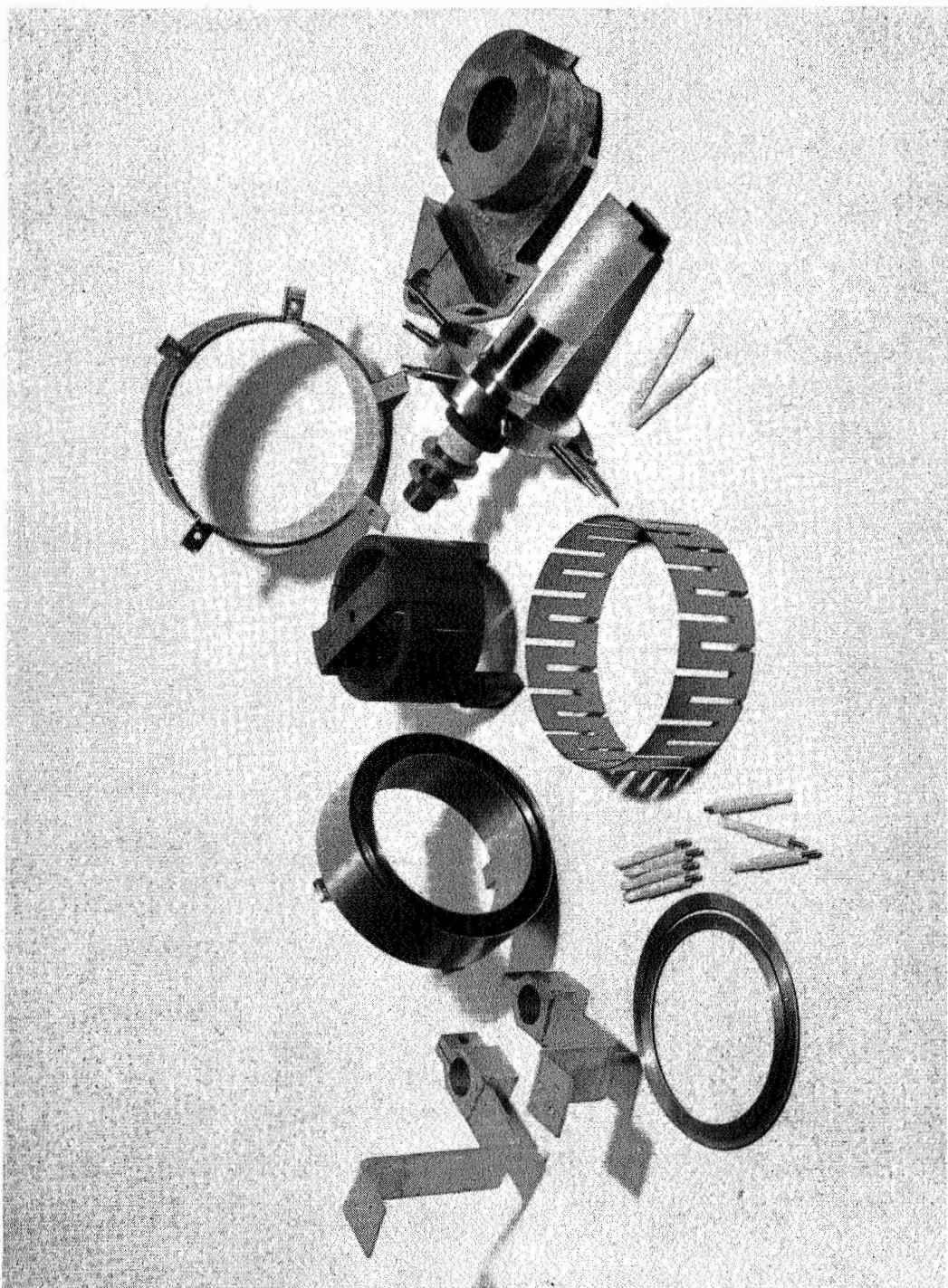


Figure 23  
COMPONENTS OF EVAPORATOR SOURCE CONFIGURATION

R-23,910  
Neg. 8716-2

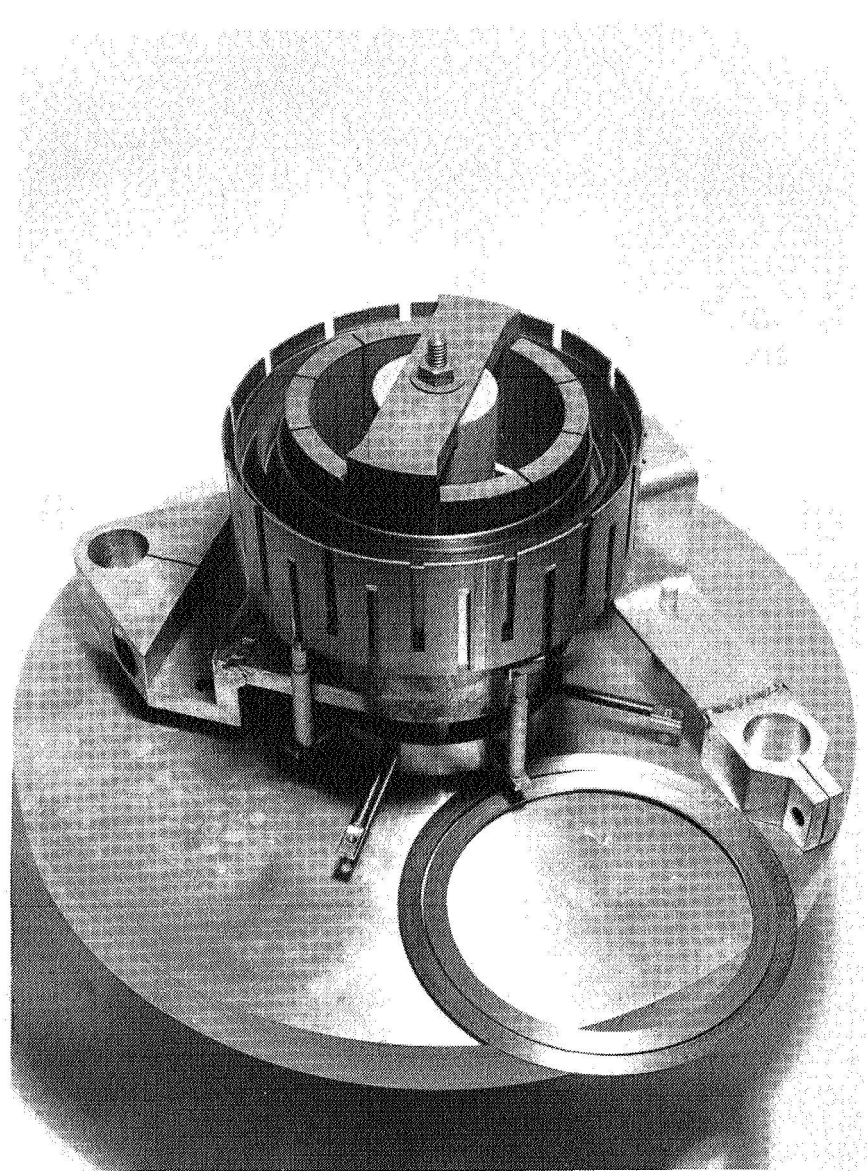


Figure 24  
ASSEMBLED EVAPORATOR SOURCE CONFIGURATION

R-23,909  
Neg. 8716-1

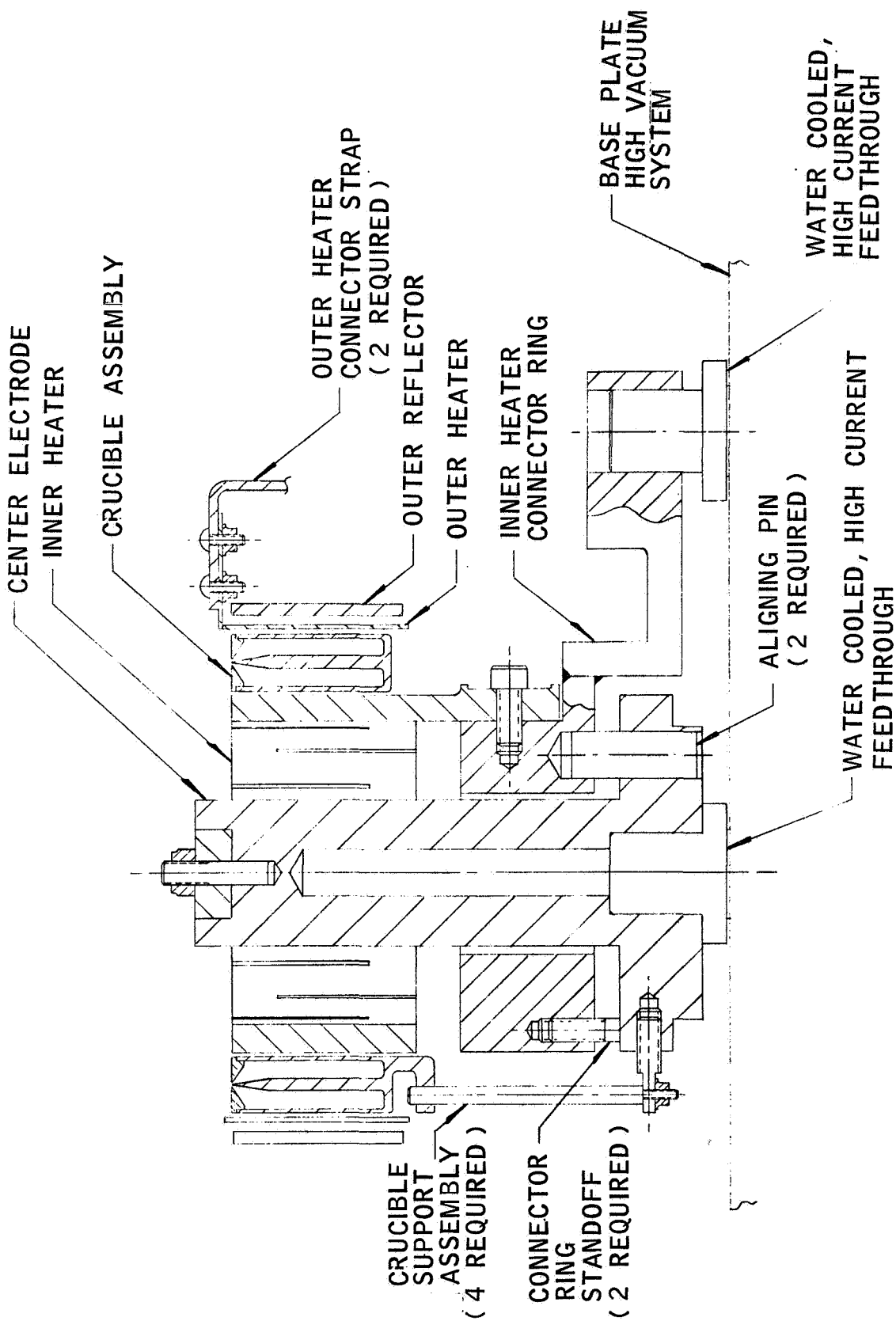


Figure 25  
EVAPORATION HEATER SOURCE

EXPERIMENTAL WORK

The production ZnSe films in vacuum was attempted by two methods: by evaporating the compound simultaneously with one element, alternatively, by coevaporation of the two elements from separate sources.

The first method involves much higher temperature for a much lower vapor density than with the second and than with the second and therefore implies difficulties in growing films of suitable thickness.

In the second method, adequate vapor density is achievable at much lower temperature but at low temperature, Se is mostly hexatomic.

Since condensation of ZnSe is only possible when equal concentration is achieved, large excess of Se or Zn will prevent formation of the compound on the substrate, and the rate of film deposition will be proportional to the lowest concentration.

The experimental work was performed in the two methods, by using 2 coaxial sources, with symmetry of revolution, and a common Knudsen's aperture, in the form of a single coaxial gap corresponding to a total area of evaporation of  $6.28 \text{ cm}^2$ .

The structure of the sources is such that they can operate at different temperatures without interaction between each other.

In either method of film deposition, the source containing the selenium is provided within its annular trough with a thin tungsten filament heated by an independent power source, at a temperature well above the temperature of the melt.

The heat of sublimation  $H_s$  of the monomer provided to the vapor by the tungsten filament is obtained from the cycle.

$$H_s(\text{Se}_x) = 2 H_s(\text{Se}) - D_o(\text{Se}_x) \text{ Kcal mole}^{-1}$$

with  $D_o$  the dissociation energy \*

$$H_{s(x)} \quad **$$

\* A.G. Gaydon, Dissociation Energies Chapman & Hall Ltd. London 1953

\*\* D.R. Stull & G.C. Sinke Vol. 18 Adv. Chemistry Series Am. Chem. Soc.

The heat removed from the filament by conduction through the gas is proportional to the filament area and its temperature. With  $D_o$  in the vicinity of 3.5 e.v. the surface of the filament would impose some restriction on the gas flow through the Knudsen's gap. In order to minimize the size of the filament and operate at temperature where the vapor pressure from the filament itself can be completely neglected a small potential is applied between the trough and the filament. The dissociation of the hexamer results therefore from a double process of surface ionization and an electron collision process.

CHEMISTRY OF II-VI COMPOUNDS

The third law method has been applied in obtaining the compounds vaporization constants from the solid-gaseous reaction. All II-VI compounds melt at high temperatures and it is generally admitted that, at the melting point, the chalcogenes are dimeric, hence the reaction is written, taking Zn Te as example,



with the equilibrium constant for the reaction

$$K_p = P_{\text{Zn}} P_{\text{Te}}^{\frac{1}{2}} \quad (2)$$

The vapor pressure  $P_{\min}$  over the congruently subliming compound i.e., when the composition is stoichiometric, is related to the equilibrium constant  $K_p$ , by

$$P_{\min} = \frac{3}{2}^{\frac{1}{2}} \frac{1}{2}^{\frac{1}{3}} K_p^{\frac{1}{3}} \quad (3)$$

where  $K_p$  is obtained from Gibbs' relation

$$G_T = H_T - TS_T$$

$$G_T = RT \ln K_p$$

$$\text{or, } \log K_p = - \frac{\Delta f_{ef} + \frac{\Delta H_T}{T}}{4.576} \quad (4)$$

with

$$f_{ef} = \frac{1}{T} \int_{298}^T C_p dT - \int_{298}^T \frac{C_p dT}{T} - S_{298} \quad (5)$$

The  $\Delta$ 's in (4) represent the difference in free energy and enthalpy between the values obtained for the gaseous and solid phases. The heat capacity  $C_p$  was calculated from Kubashewski's method \*.

Since the total vapor pressure in the dimeric case is:

$$P = p_{Zn} + p_{Te_2}$$

we have,

$$p_{Zn} = p_{Te_2}^{1/3} K_p^{1/3} \quad (6)$$

In correlating vapor pressures with Knudsen's diffusion method, for the source described in Appendix I, for any species  $i$ , of mass  $M_i$ , with mass spectrometry data, with,

$$p_i = N_i (2\pi k T M_i)^{1/2} \text{ cm}^{-2} \text{ sec}^{-1}$$

\* O. Kubashewski, E. Evans Metall. Thermochem. Pergamon Press 1958

with  $N_i$ , obtained from the ratio of ions  $i I^+$  current, to electrons current  $I$ , from,

$$N_i = \frac{i^+ L^2}{\gamma Q A I}$$

with  $\gamma$ , a constant, measured for the Vecco unit used in these measurements, which lumps together numerical constant, length of electrons trajectory and factor of ions collection. The steradiancy is taken into account with  $A$  the area of the source,  $L$  distance from the source;  $Q$  the ions cross section, was taken as,

$$\text{Zn in covalent state} \quad Q_{Zn} = 16 \times 10^{-16} \text{ cm}^2$$

$$\text{Te in same s. p state} \quad Q_{Te} = 25.6 \times 10^{-16} \text{ cm}^2$$

by weight loss method, with:

$$W = 5.83 \times 10^{-2} P_i \left(\frac{T}{M_i}\right)^{1/2} \text{ cm}^{-2} \text{ sec}^{-1}$$

in both methods, one must take into account the complex conductance of the coaxial cell, which is the sum of the conductances, (1) from the circular trough and, (2) from the circular gap with,

$$C = \frac{C_1 C_2}{C_1 + C_2}$$

The conductance of our cell was calculated from kinetic theory of gases, for example, by considering an element of length  $dL$  of the trough, of constant cross section  $A$ , and perimeter  $B$ , with  $v$  the flow speed it follows that,

$$V = A v$$

$$\text{or,} \quad Q = PV = PA v \quad (7)$$

the force  $dF$  acting on an element of volume  $V$ , is

$$dF = AdP \quad (8)$$

the number of collisions  $\nu$  per unit area and time, from the evaporating molecules is,

$$\nu = \frac{1}{4} n v_a$$

with  $v_a$ , the mean arithmetic velocity.

$$v_a = \left( \frac{8 kT}{\pi M_i} \right)^{1/2}$$

since from the equation of states

$$N = \frac{P}{k T}$$

$\nu$  becomes,

$$\nu = \frac{1}{4} \frac{P}{k T} \left( \frac{8 kT}{\pi M_i} \right)^{1/2}$$

and the quantity of motion transmitted

$$\begin{aligned} &= BdL \nu M_i v_a \\ &= BdL \frac{P}{(\frac{\pi k T}{2})^{1/2}} M_i v_a \end{aligned}$$

which, equated with the force (8) gives

$$AdP = \frac{BdL P v_a}{2 \left( \frac{\pi k T}{2M_i} \right)^{1/2}} \quad (9)$$

eliminating  $P v_a$  between (7) and (9)

$$AdP = \frac{BdL Q}{2 A \left( \frac{\pi kT}{2 M_i} \right)^{1/2}}$$

and,

$$C = \frac{Q}{dP} = 2\pi \left( \frac{kT}{2\pi M_i} \right)^{1/2} \frac{A^2}{BdL}$$

or, more precisely with  $8/3$  substituted for  $\pi$ , with a length L, Figure 26,

$$C = \frac{16}{3} \left( \frac{k T}{2\pi M_i} \right)^{1/2} \frac{A^2}{BL} k \quad \text{c.g.s.} \quad (10)$$

with Clauising's correction factor  $k$ , given Table I with the source area,  $A = \frac{\pi}{4} (D_1^2 - D_3^2)$  et, the source perimeter  $B = \pi (D_1 + D_3)$  eq. (10) becomes,

$$C = \frac{\pi}{3} \left( \frac{k T}{2\pi M_i} \right)^{1/2} \frac{(D_1^2 - D_3^2)^2 k}{(D_1 + D_3) L} \quad (11)$$

since, from the equation of states,

$$N = \frac{PV}{kT} = \frac{Q}{kT}$$

lumping together, numerical coefficients and geometric factors, in the form of a constant, we can write (11) as

$$N_i = \frac{ct. \left( \frac{T}{M_i} \right)^{1/2} \frac{P_i}{kT}}{kT} = \alpha \frac{P}{T^{1/2}} \quad (12)$$

the same procedure applies for any part of the source where the conductance is sought.

Applying this approach to the complex conductance of the source schematized Figure 26, for the experimental determination of  $P_{min}$  (eq. 1) has yielded the values plotted in Figure 27. These results are closer to the values published by (Ref.\*\*) than those previously given in (Ref.\*\*\*).

TABLE I

Clausing's Correction factor for source geometry

$r_3/r_1$	0	0.1	0.2	0.3	0.4	0.5	0.6	0.7	0.8	0.9	0.95	0.977
k	1	1.04	1.065	1.09	1.11	1.15	1.2	1.25	1.34	1.49	1.6	1.7

Ref. \*\* R.A. Reynolds, D.G. Stroud, D.A. Stevenson J. Electro. Chem. Soc.  
114.1281.1967

Ref. \*\*\* Goldfinger & Jevnehomme WADD TR60782 Part XVIII Nov. 1963

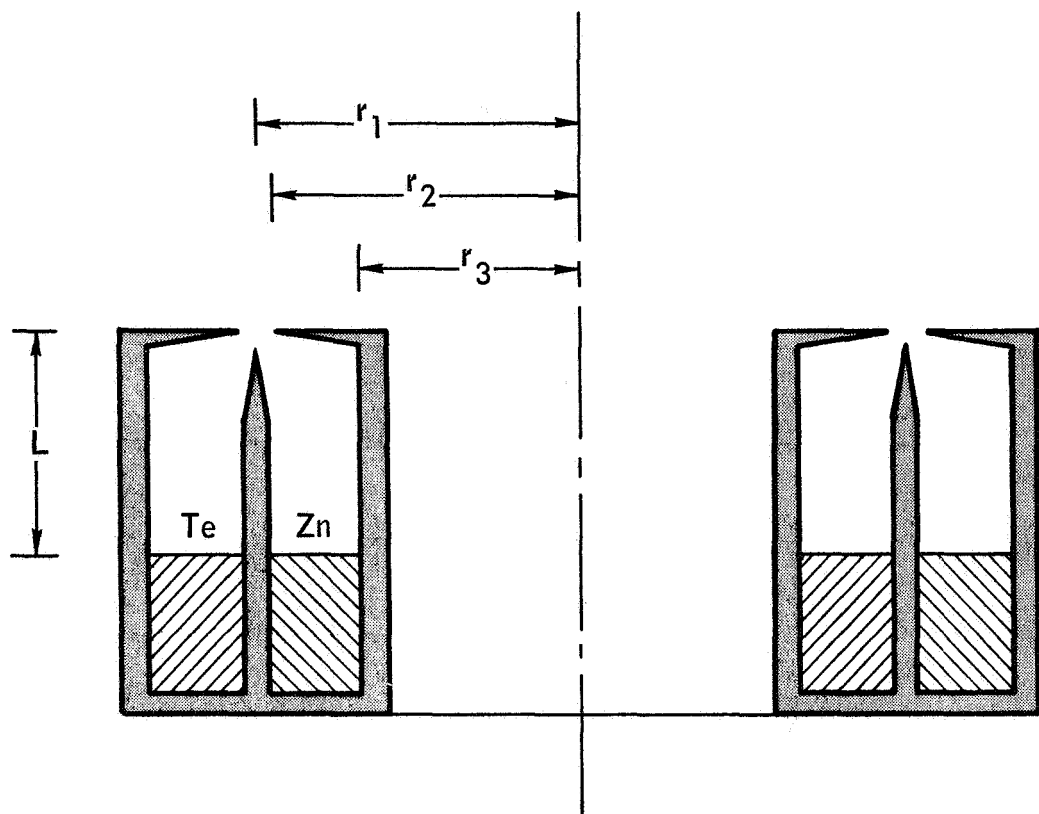


Figure 26  
COAXIAL CIRCULAR SOURCES

R-26,769

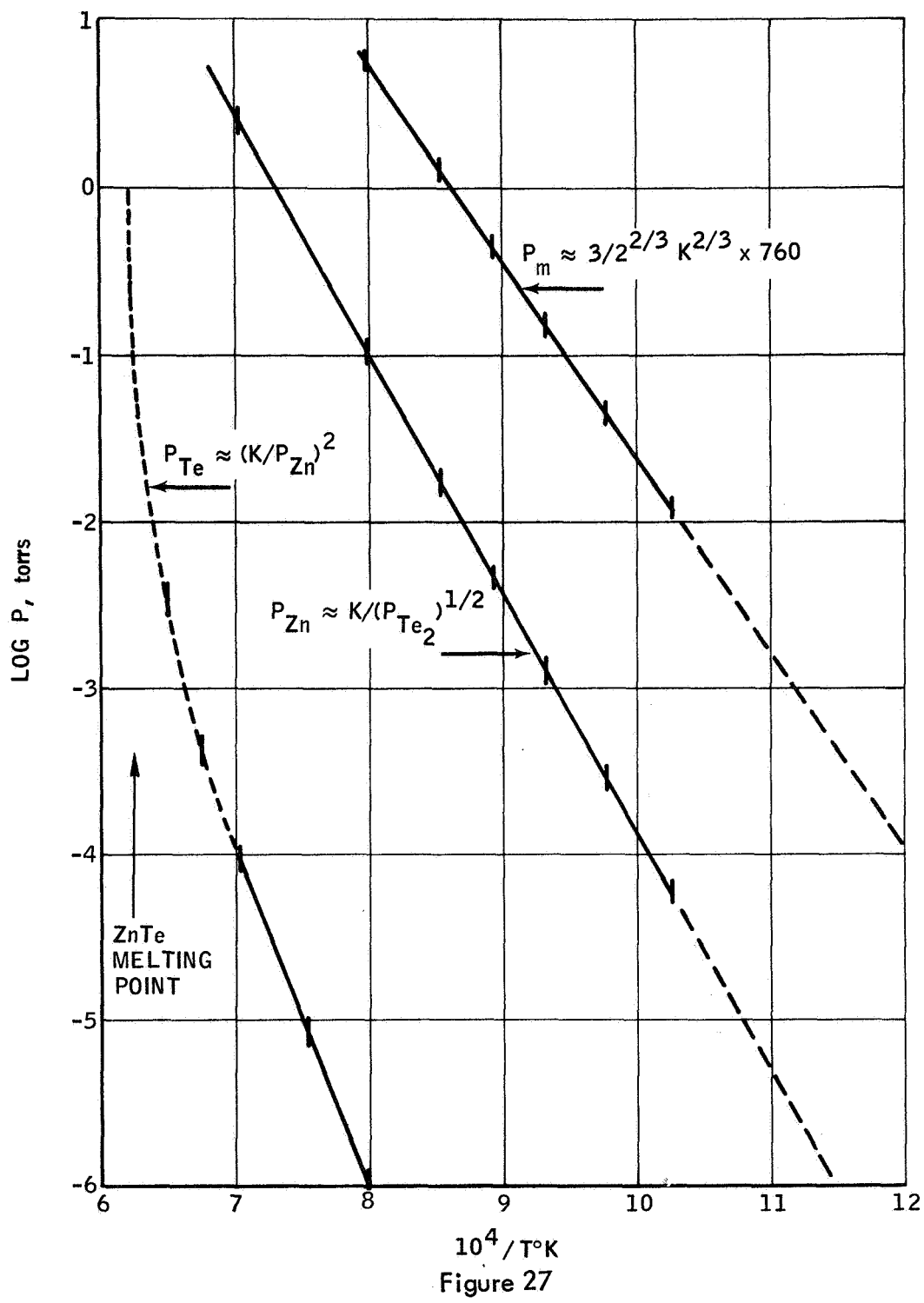


TABLE II  
 SUBLIMATION AND PARTIAL PRESSURES OF ZnSe

T <sup>o</sup> C	P <sub>min</sub>	P <sub>Zn</sub>	P <sub>Se<sub>2</sub></sub>	P <sub>ZnSe</sub>
749	3.15 10 <sup>-3</sup>	2.1 10 <sup>-3</sup>	1 10 <sup>-3</sup>	4.6 10 <sup>-9</sup>
779	8.25 10 <sup>-3</sup>	5.5 10 <sup>-3</sup>	2.7 10 <sup>-3</sup>	8.3 10 <sup>-8</sup>
801	1.89 10 <sup>-2</sup>	1.26 10 <sup>-2</sup>	6.3 10 <sup>-3</sup>	1 10 <sup>-6</sup>
844	3.45 10 <sup>-2</sup>	2.3 10 <sup>-2</sup>	1.1 10 <sup>-2</sup>	6 10 <sup>-6</sup>
876	6.75 10 <sup>-2</sup>	4.5 10 <sup>-2</sup>	2.2 10 <sup>-2</sup>	4.5 10 <sup>-5</sup>
917	1.24 10 <sup>-1</sup>	8.3 10 <sup>-2</sup>	4.15 10 <sup>-2</sup>	2.8 10 <sup>-4</sup>
946	1.93 10 <sup>-1</sup>	1.29 10 <sup>-1</sup>	6.2 10 <sup>-2</sup>	1 10 <sup>-3</sup>

The values given above are in addition to the values plotted in Figure 7.

REFERENCES

1. A. N. Nesmeyanov, "Vapor Pressure of the Elements", Academic Press (1963).
2. D. R. Stull and G. C. Sinke, Adv. in Chem. Series #18 Amer. Chem. Soc. (1956)
3. M. Kabayashi, Intern. Z. Metallog., 2-65. (1912)
4. J. Carides and A. G. Fisher, Solid State Comm., 2-217 (1964)
5. A. G. Fisher, J. Electrochem. Soc., 106-838 (1959)
6. S. Narita, H. Harada, K. Nagusaka, J. Phys. Soc. Japan, 22-1176 (1967)
7. L. C. Greene, D. C. Reynolds, S. J. Czysack, W. M. Baker, J. Chem. Phys., 29-1375 (1958)
8. W. W. Piper, S. J. Polish, J. Appl. Phys., 32-1278 (1961)
9. M. Aven, W. Garwacki, J. Electrochem. Soc., 110-401 (1963)
10. D. B. Holt, Brit. J. Appl. Phys., 17-1395 (1966)
11. H. M. Manusevit, J. Electrochem. Soc., 115-434 (1968)
12. Swanson & Fuyat, NBS Circular 539, Vol. III (1953)
13. NBS Monograph, 25-3 (1964) Spinulescu-Carnaru Phys. Status Solidus, 18-269 (1966)
14. Geological Survey Circular, 29 August (1948)
15. H. Kedesy, Am. Min., 39-750 (1954)
16. H. P. Klug, L. E. Alexander, X-ray Diffraction Procedure, J. Wiley (1954)
17. S. Ino, D. Watanabe, S. Ogawa, J. Phys. Soc. Japan, 19-881 (1964)
18. K. V. Shalimova, A. F. Andrushko, J. Dima. Sov. Phys. Cryst., 10-414 (1966)
19. M. Aven, D. N. Cook, J. Appl. Phys., 32-960 (1961)
20. M. Aven, Appl. Phys. Letters, 7-146 (1965)
21. M. Aven, W. Garwacki, J. Appl. Phys., 38-2302 (1967)
22. S. Larack, R. Schruder, C. Stocker, Phys. Rev., 108-587 (1957)
23. M. Aven, Appl. Phys. Letters, 7-146 (1965)
24. M. Aven, B. Segall, Phys. Rev., 130-87 (1963)
25. A. G. Fisher, Phys. Letters, 12-313 (1964)
26. H. K. Henish, Rectifying Semiconductor Contacts, Clarendon Press (1957)
27. A. N. Georgobiani Opt. Spectry (USSR) Eng. Transl., 11-231 (1961)
28. M. Aven, D. A. Cusano, J. Appl. Phys., 35-606 (1964)
29. R. H. Bube, Photoconductivity of Solids, J. Wiley (1960)
30. G. Giesecke, Semiconductors, Vol. 2, Academic Press (1966)